Shark Skin Inspired Micro Structural Design To Improve Aerodynamic Performance

By

Project Member

Prawin Raj P - 211419114216

Batch No: 08

Under the Supervision

Of

Mr. I. JOHN SOLOMON M.E., (PhD).,

Assistant Professor

Department of Mechanical Engineering

Panimalar Engineering College

Shark Skin Inspired Micro Structural Design To Improve Aerodynamic Performance

- Prawin

Objective

Purpose of the project

- There have been significant efforts recently aimed at improving the aerodynamic performance of aerofoils through the modification of their surfaces. Inspired by the drag-reducing properties of the tooth-like denticles that cover the skin of sharks, I described here the simulation-based investigations into the aerodynamic effects of novel denticle-inspired designs placed along the suction side of an aerofoil.
- Through parametric modelling to query a wide range of different designs, I discovered a set of denticle-inspired surface structures that achieve simultaneous drag reduction and lift generation on an aerofoil, resulting in lift-to-drag ratio improvements comparable to the best-reported for traditional low-profile vortex generators and even outperforming these existing designs at low angles of attack.
- Such behavior is enabled by two concurrent mechanisms: (i) a separation bubble in the denticle's wake altering the flow pressure distribution of the aerofoil to enhance suction and (ii) streamwise vortices that replenish momentum loss in the boundary layer due to skin friction.

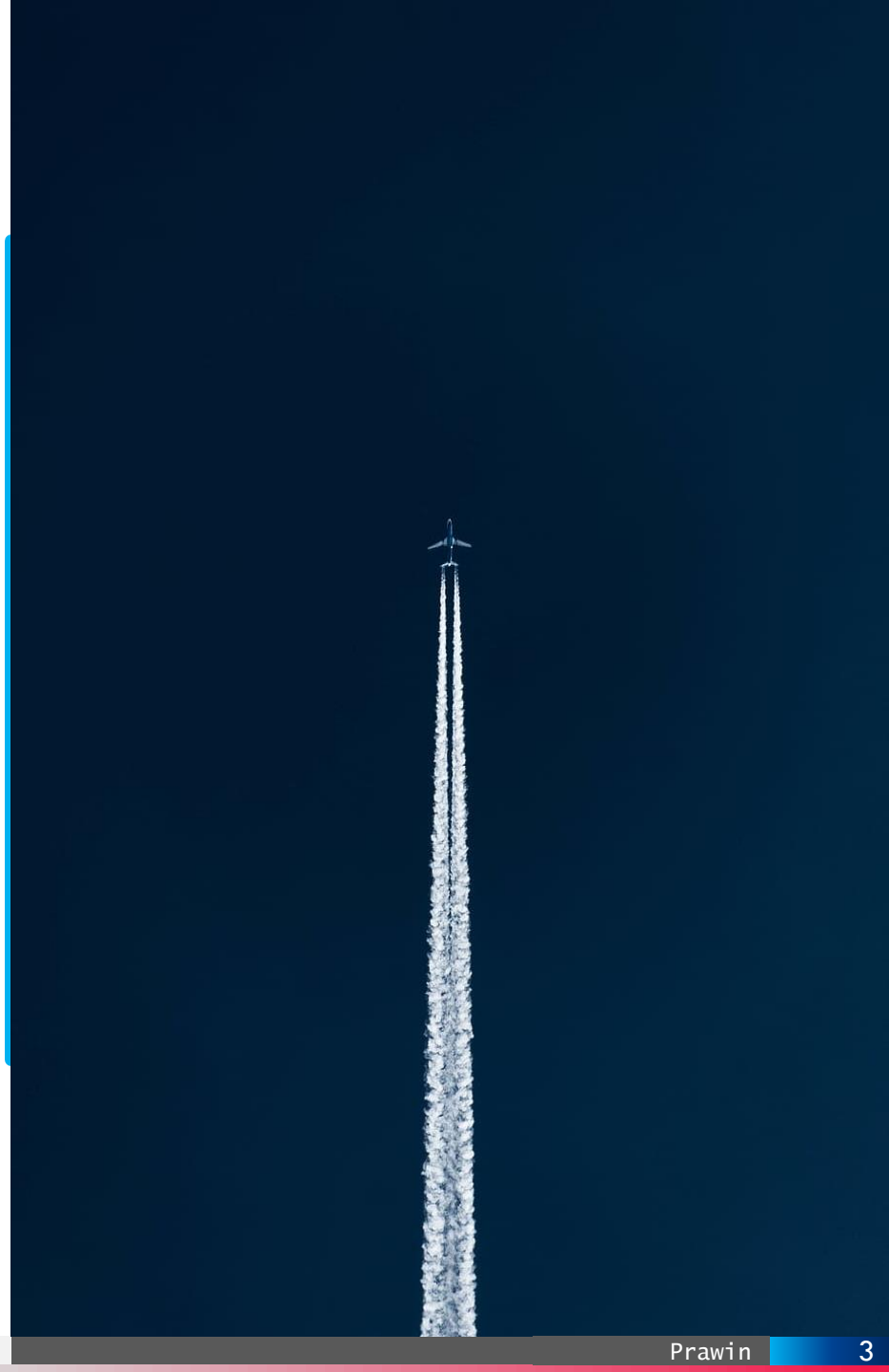

Introduction

- Systems that move suspended within a fluid, such as airplanes, wind turbines, drones and helicopters, all benefit from increased lift-to-drag ratios which results in lower energy consumption. Motivated by this need, two main strategies have been proposed to maximize the lift and minimize the drag.
- On one hand, several active flow control methods, which involve the addition of auxiliary power into the system, have been demonstrated for both drag reduction and lift augmentation. On the other hand, it has also been shown that passive flow control strategies based on geometric modifications are capable of altering lift and drag.

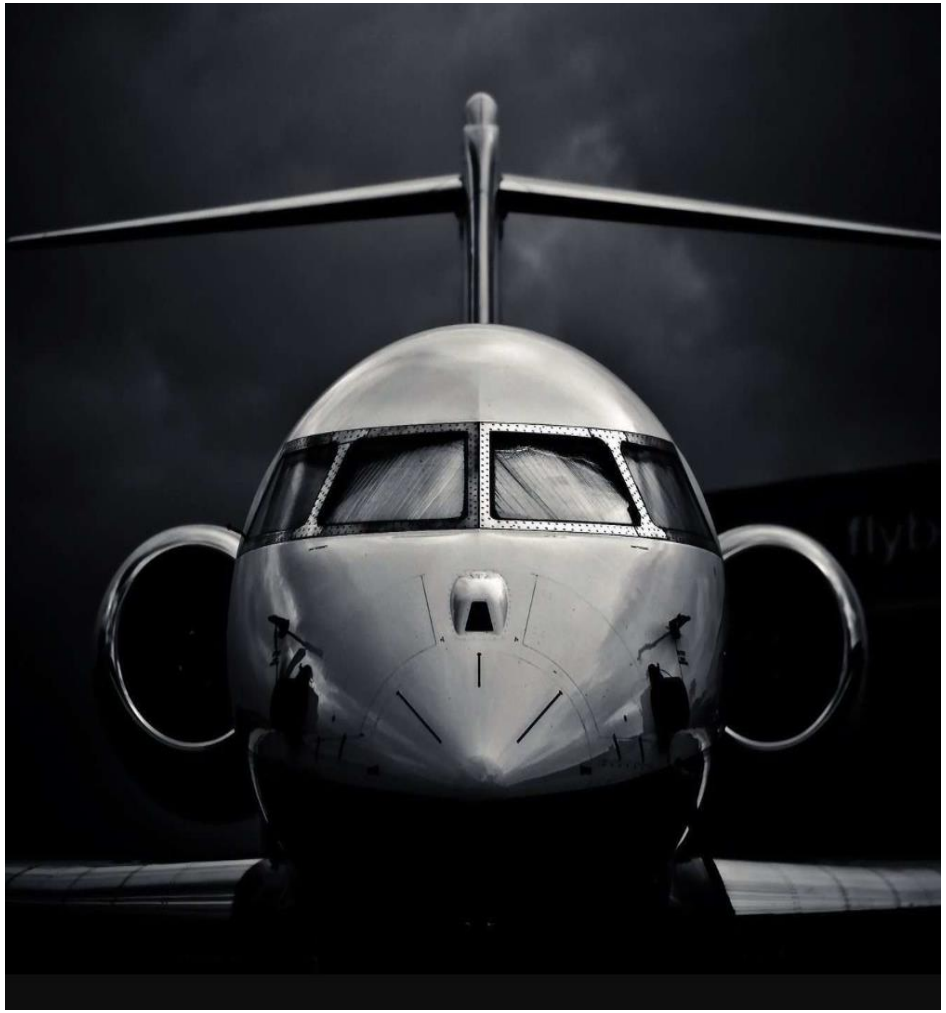

- These include vortex generators, Gurney flaps and winglets, which reduce drag and increase lift by passively altering the flow to favorably affect the pressure gradients along the aerofoil.
- Although active methods typically yield better results than the passive ones, they require the supply of external energy, and in fully automated systems rely on complex sensor technology and algorithm development. By contrast, passive techniques are easy to implement and free from any kind of external energy requirements.

- Nature, through the course of evolution, has arrived at structures and materials whose traits often offer inspiration for the design of synthetic systems with unique properties. Specifically, biological systems have evolved a wide range of drag reducing mechanisms that have inspired the design of synthetic surfaces.
- Shark skin is one such example and is covered with rigid bony denticles (or scales) that exhibit a plate-like upper section with ridges, which narrows to a thin neck that anchors into the skin.
- These intricate structures have inspired the development of several drag reducing surfaces, ranging from highly simplified ridge-like geometries to complex three-dimensional (3D) printed models that replicate the structural complexities of individual denticles.
- These denticle-inspired surfaces have resulted in a drag reduction of 10% compared to corresponding smooth control surface.

Literature Survey

- "Shark skin as a biomimetic model for the reduction of aerodynamic drag in vehicles" by R. Kesel, M. Herrmann and M. Scherge. This paper explores the structure and properties of shark skin, and discusses how biomimetic designs inspired by the skin can be used to improve the aerodynamic performance of vehicles.
- "Biomimicry of shark skin and cetacean flippers for reduction of flow-induced noise and drag" by C. M. Sayer and S. A. Megill. This paper discusses the use of biomimetic designs based on shark skin and cetacean flippers to reduce flow-induced noise and drag in engineering applications.
- "The shark skin effect: reducing aircraft drag" by T. J. Geoghegan and J. J. Leahy. This paper investigates the potential of shark skin inspired designs to reduce aircraft drag, and discusses the challenges and opportunities associated with this approach.
- "Shark skin-inspired surfaces for fluid-drag reduction in turbulent flow regimes" by K. Bhushan and Y. C. Jung. This paper presents a comprehensive review of research on shark skin inspired surfaces for fluid-drag reduction in turbulent flow regimes, including experimental studies and numerical simulations.
- "Biomimetic shark skin: design, fabrication and hydrodynamic function" by J. W. H. Yong, H. Y. Low and C. S. Tan. This paper describes the design and fabrication of biomimetic shark skin surfaces, and investigates their hydrodynamic function in a range of flow conditions.
- "Biomimetic shark skin: a review of design principles and potential applications" by S. A. Megill and C. M. Sayer. This paper provides a comprehensive review of the design principles and potential applications of biomimetic shark skin, including the development of coatings, surfaces and materials for a range of engineering applications.

Hypothesis

Concept to design

- We focus on aerofoils and investigate experimentally how 3D models of shark denticles arranged on their suction side can change fluid flow passively. While previous research has primarily focused on the effect of shark denticles on drag reduction, we show that the denticles can both enhance lift and reduce drag, resulting in high lift-to-drag ratios.
- (1) Environmental scanning electron microscope (ESEM) image of denticles from a shortfin mako shark used in this study (scale bar: 200µm), and (2) its corresponding parametric 3D model. (3,4) These denticles were arranged on the suction side of a NACA0012 aerofoil in a variety of different configurations, two of which are shown here. (5) All of the aerofoils were then tested in fluid flow to see how the denticles will affect lift and drag.

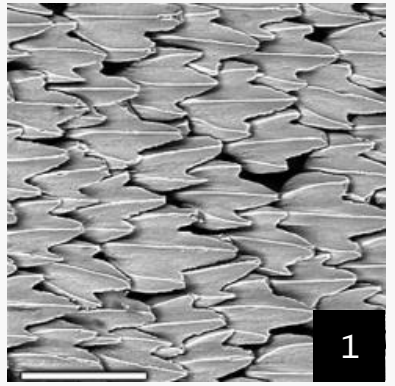

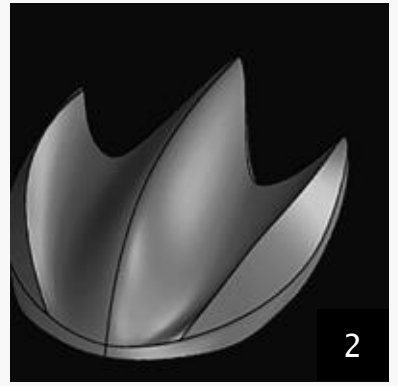

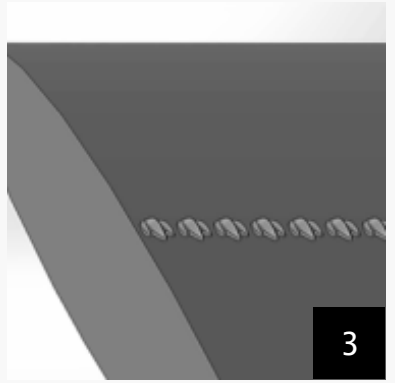

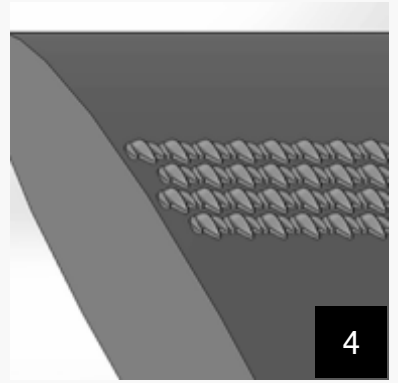

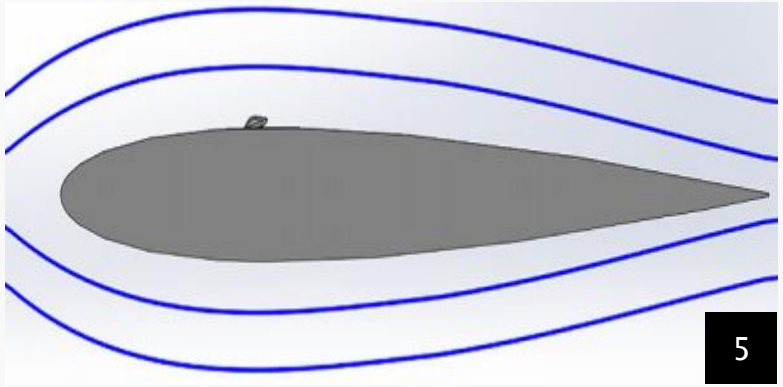

Working

- We investigate the mechanisms underlying this behavior and discover that shark denticles generate both a recirculation zone (in the form of a short separation bubble in the wake of the denticle) that changes the pressure distribution of the aerofoil to improve suction and streamwise vortices that reduce drag by replenishing momentum to the flow that would otherwise be lost due to skin friction.
- We looked at a symmetric NACA0012 aerofoil with an aspect ratio of W/L = 2.8 (L = 68 mm for the chord length and W for the span length). We arranged 3D representative models of a shark denticle on its suction side, based on micro-computed tomography (micro-CT) scans of denticles from Isurus oxyrinchus (Through Article).

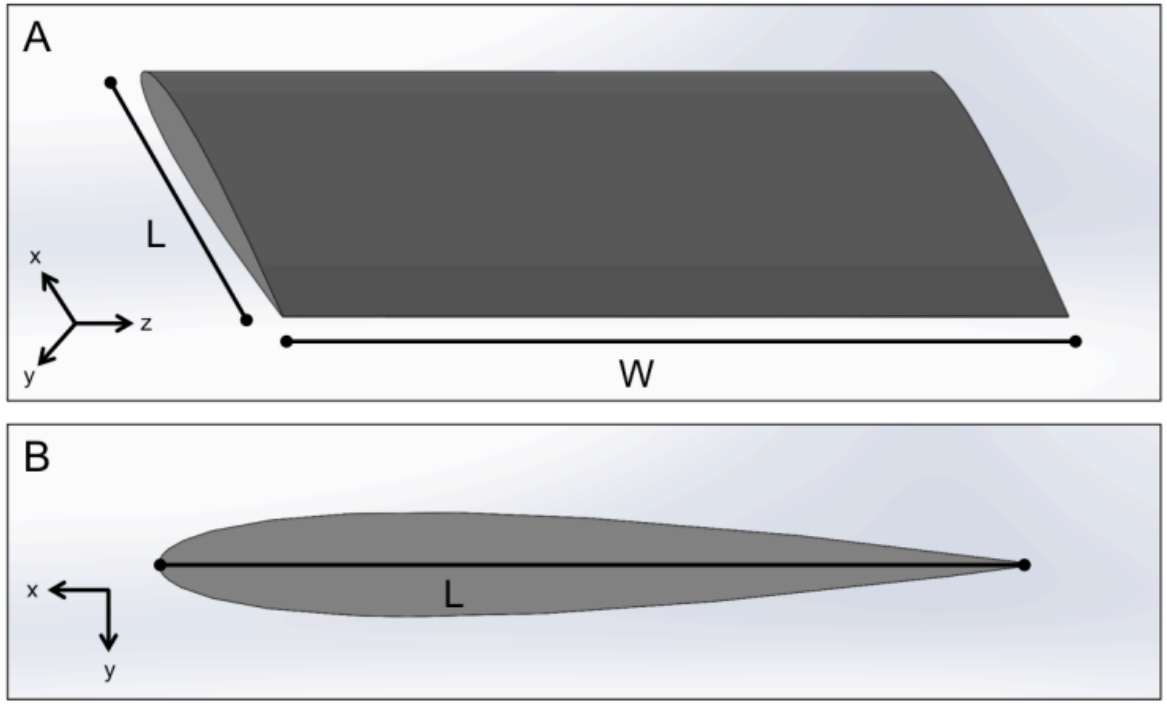

Experimental Setup

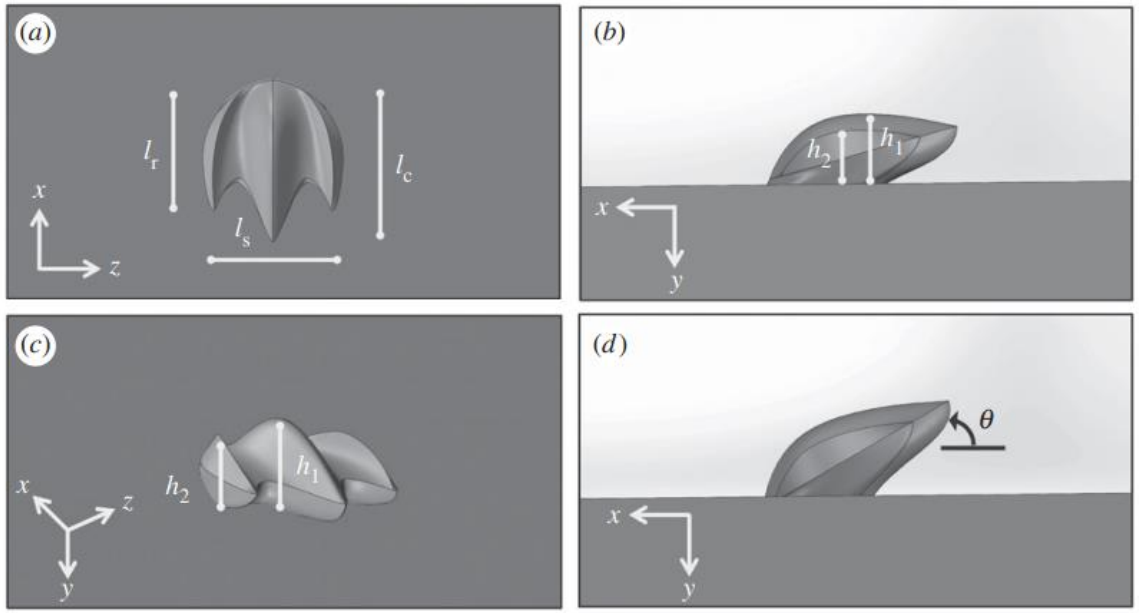

- The chordwise length of the middle ridge (lc), the chordwise length of the side ridges (lr), the spanwise length between the outside ridges (ls), the height of the middle ridge (h1), the height of the side ridges (h2), and the tilt angle(θ) are the geometric parameters.
- We created 20 aerofoils with different arrangements (including either single or multiple rows of denticles), sizes, and tilt angles of these denticles in order to physically explore the parameter space as much as possible and to converge on the best design. In our study, we kept lc/ls = 1.37, lc/lr = 1.25, h1/h2 = 1.40, and lc/h1 = 2.95 constant for all foils based on shark denticle measurements.

• The 3D parameterized model of a single representative denticle from a shortfin mako shark (Isurus oxyrinchus) was constructed using a micro CT scanner (XradiaVersaXRM-500, at Cornell University, Institute of Biotechnology) and meshed using Mimics 3D (Materialize Inc., Leuven, Belgium).

• (A) Side view of the foil showing the chordwise placement of the denticles on its suction side. (B) Foils #1 - #13 have a single row of denticles with a spanwise separation b. (C)-(D) Foils #14 - #20 comprise multiple rows of denticles arranged either on a (C) linear or a (D) staggered pattern.

• All denticles were placed on the suction side of the airfoils with their grooves aligned parallel to the chordwise direction 13 foils (Foils #1 - #13) comprise a single row of denticles placed at different distances.

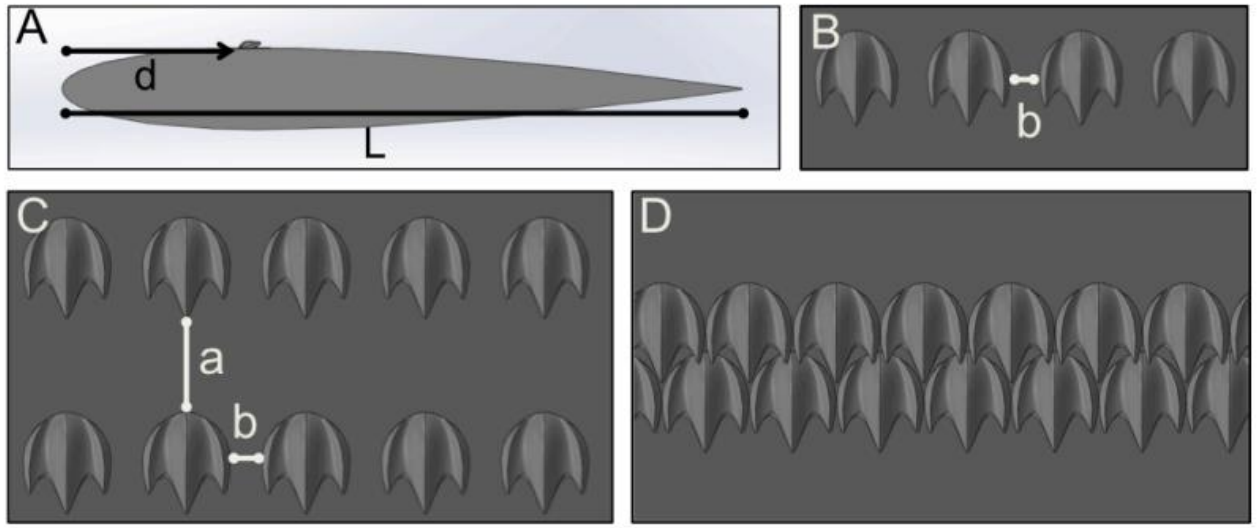

• d/L, along the chord (d denoting the distance from the leading edge to the front of the row of denticles – see Fig 5) and with a spanwise separation b varying between 0 and 3 mm.

• The remaining 7 foils (Foils #14 - #20) comprise multiple rows of denticles, arranged either according to a linear or staggered pattern.

Foil #	Pattern	# of Rows	Chordwise Separation, a [mm]	Spanwise Separation, b [mm]	Location along Chord, d/L	Size of Denticle, l_c [mm]	Tilt Angle of Denticle, θ [deg.]
1	linear	1	n/a	1	0.26	2	15
2	linear	1	n/a	1	0.16	2	15
3	linear	1	n/a	2	0.10	2	15
4	linear	1	n/a	2	0.10	4	15
5	linear	1	n/a	2	0.16	4	15
6	linear	1	n/a	2	0.26	4	15
7	linear	1	n/a	2	0.16	4	30
8	linear	1	n/a	3	0.10	6	15
9	linear	1	n/a	3	0.16	6	15
10	linear	1	n/a	0	0.26	2	15
11	linear	1	n/a	2	0.26	2	15
12	linear	1	n/a	1	0.38	2	15
13	linear	1	n/a	1	0.50	2	15
14	staggered	2	closely packed	closely packed	0.26	2	15
15	linear	2	closely packed	1	0.26	2	15
16	linear	2	1	1	0.26	2	15
17	linear	2	2	1	0.26	2	15
18	linear	4	closely packed	3	0.10	4	15
19	staggered	4	closely packed	closely packed	0.16	4	15
20	linear	26	closely packed	1	0.26	2	15

- Note that for these foils the geometric parameter d as specified in Table 1 indicates the distance from the leading edge to the front of the first row of denticles. Moreover, in Table S1 "closely packed" refers to denticles spaced as closely as possible without physically touching.

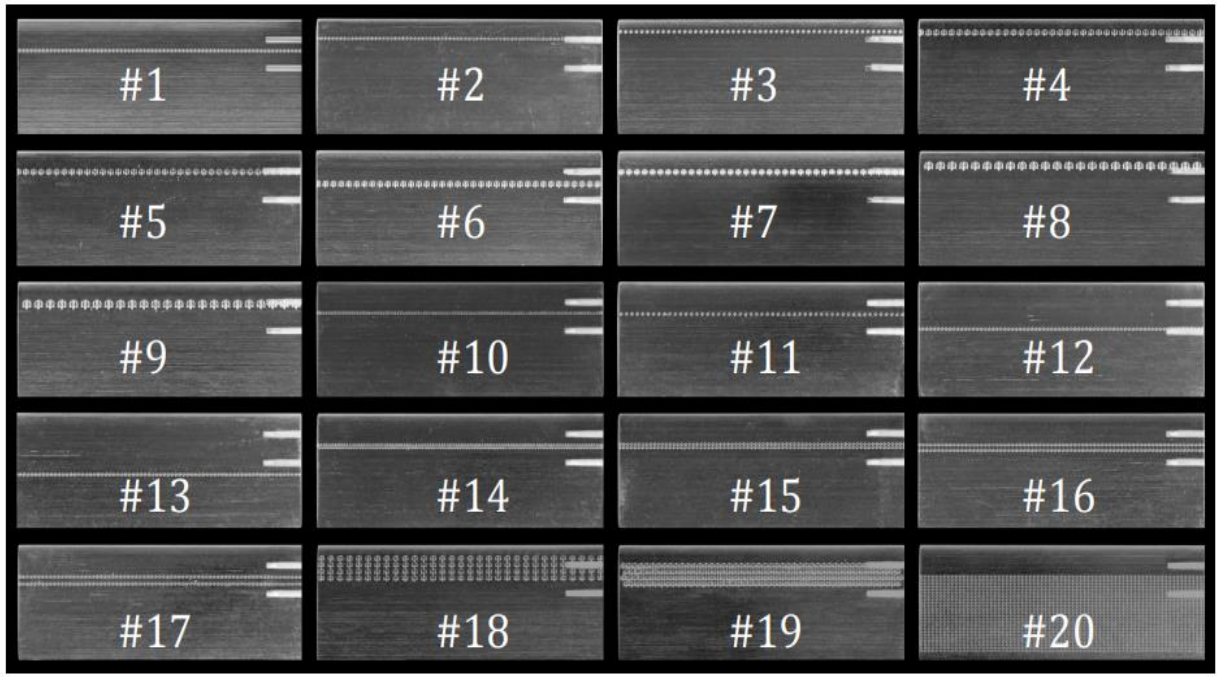

Calculation

- Given the relevant Reynolds number ranges for aerodynamic applications (less than 10000 to greater than 1000000).
- Each foil's performance was tested in steady state within air flow medium (kinematic viscosity y = 1.48 X 10-5 m2 s-1) in the laminar regime with a flow speed of U = 0.58 ms-1, which corresponds to a chord Reynolds number of Rec = UL/v ≈ 4 X 104.
- The foils were tested at angles of attack, α, from 0° to 24° (post stall and within the limits of the experimental set-up) in increments of Δα = 2°.
- At each angle, the force experienced by the foils parallel to the flow, FD, and perpendicular to the flow, FL were recorded from these measurements, the dimensionless coefficients of lift (CL) and drag (CD) were calculated as

$$C_L = \frac{2F_L}{\rho A U^2}, \quad C_D = \frac{2F_D}{\rho A U^2},$$

- Where A = W X L = 12920 mm2 is the aerofoil planform area (regardless of foil orientation) and ρ = 1.293 kg m-3 is the density of air.
- Density - Constant (ρ = 1.293 kg m-3), Flow – Coupled, Fluid – Air, Reynolds Average Navier Stokes Method, Laminar Flow, Steady State
- As at the moderate Reynolds number considered in this study, the force measurements can be quite sensitive to the different parameters of the experiment, at least six trials were conducted for each of the 20 foils and each presented data point is the average of many tests.

VARYING CHORDWISE POSITION AND SIZE OF DENTICLES

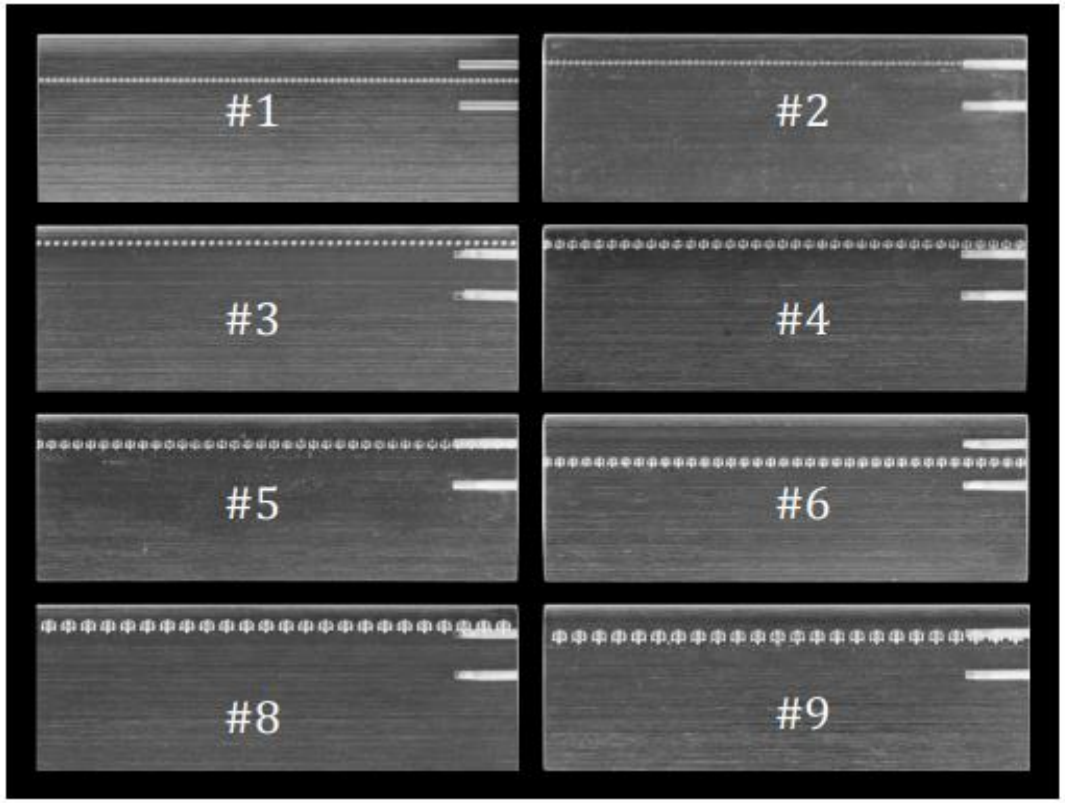

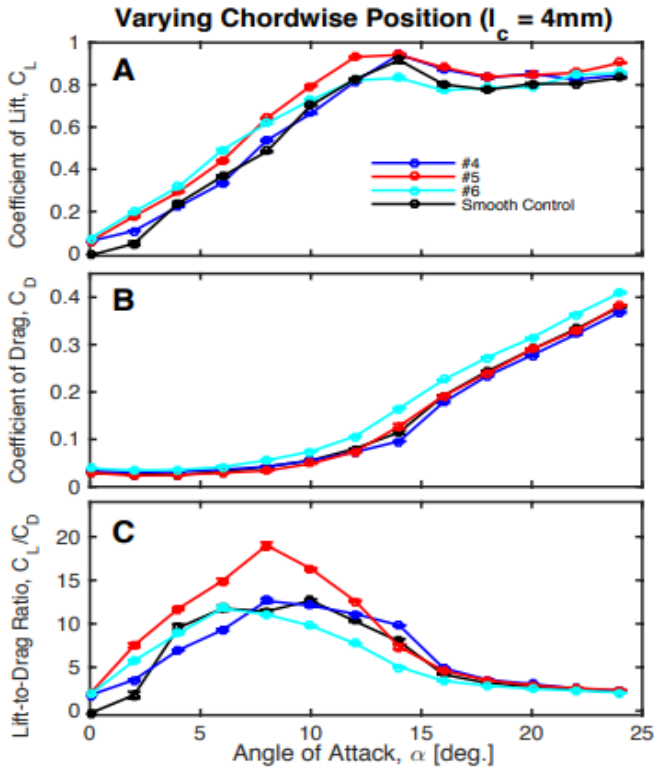

Result of Foils #4, #5 and #6

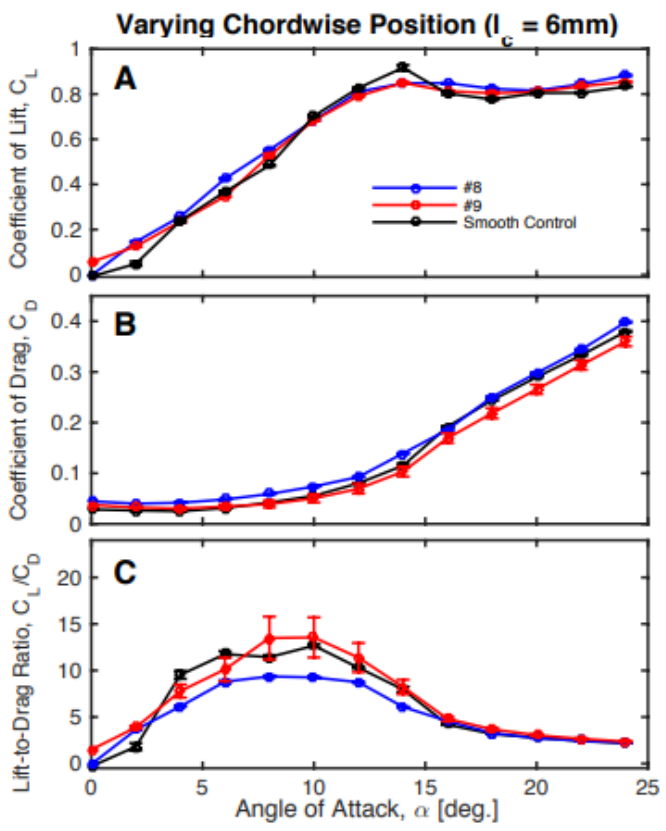

Result of Foils #8, #9

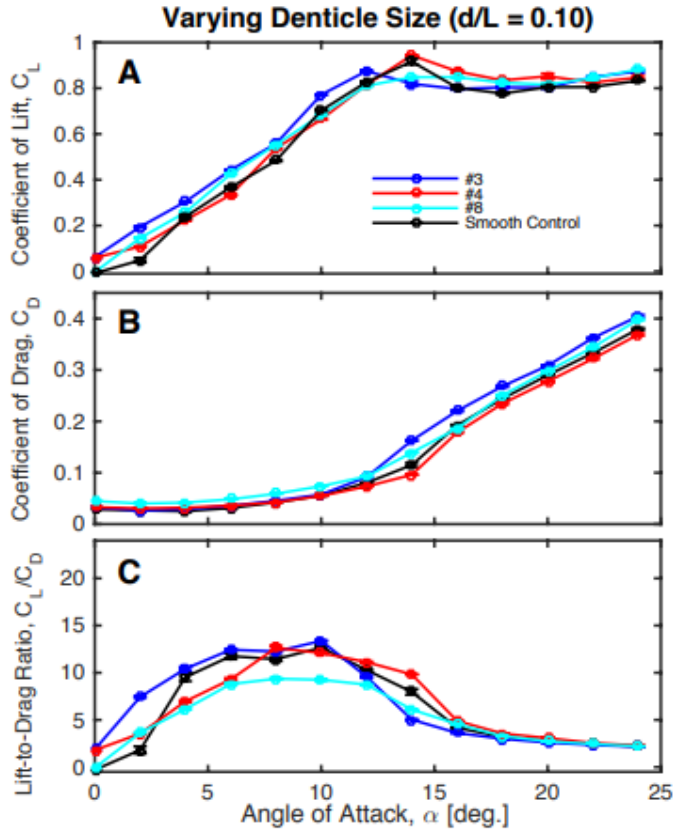

Result of Foils #3, #4 and #8

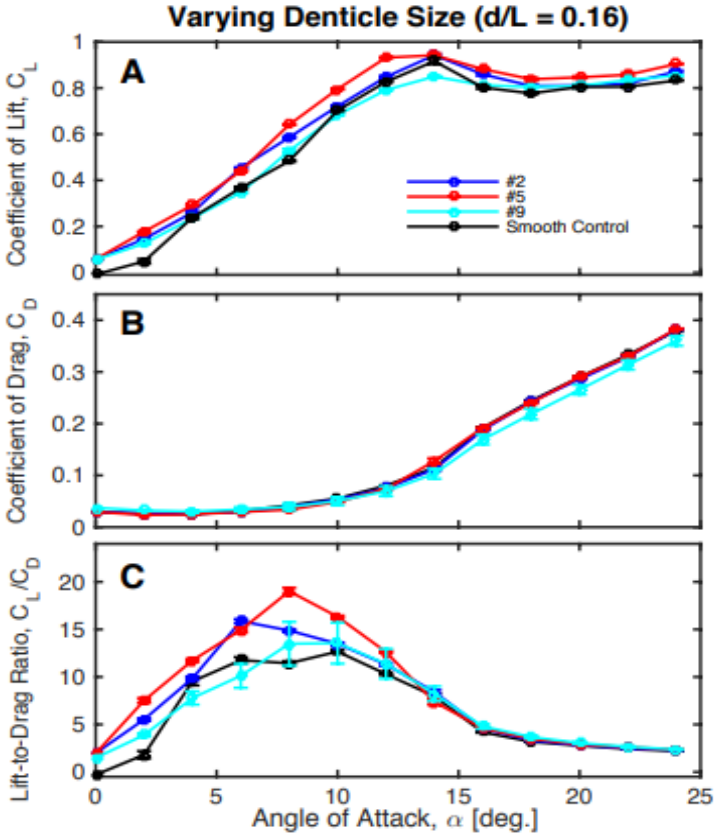

Result of Foils #2, #5 and #9

VARYING CHORDWISE POSITION

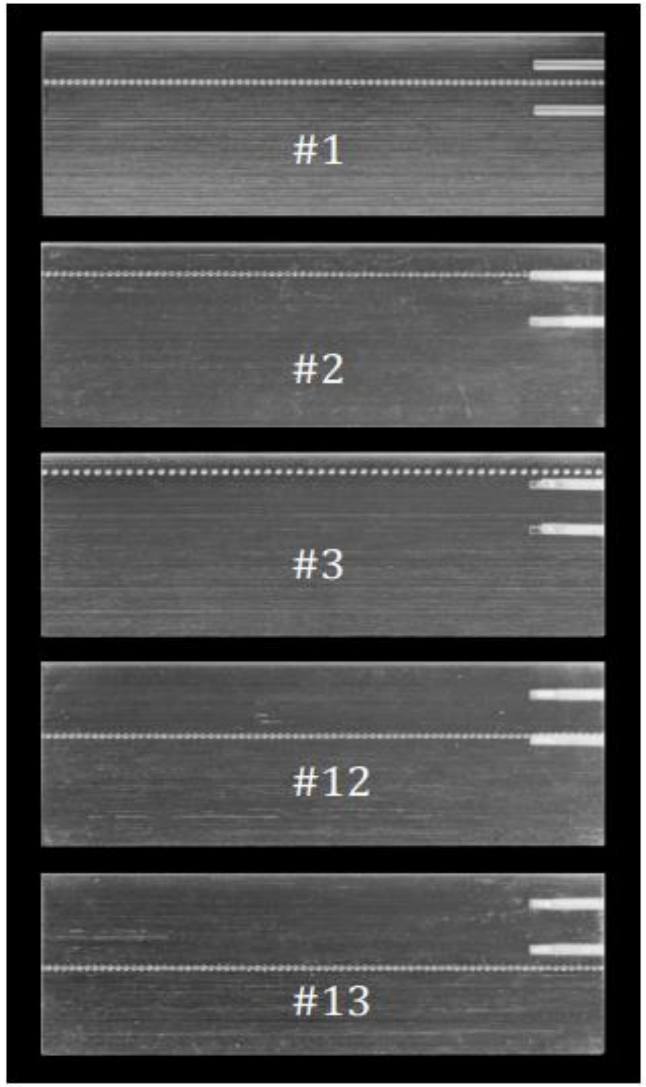

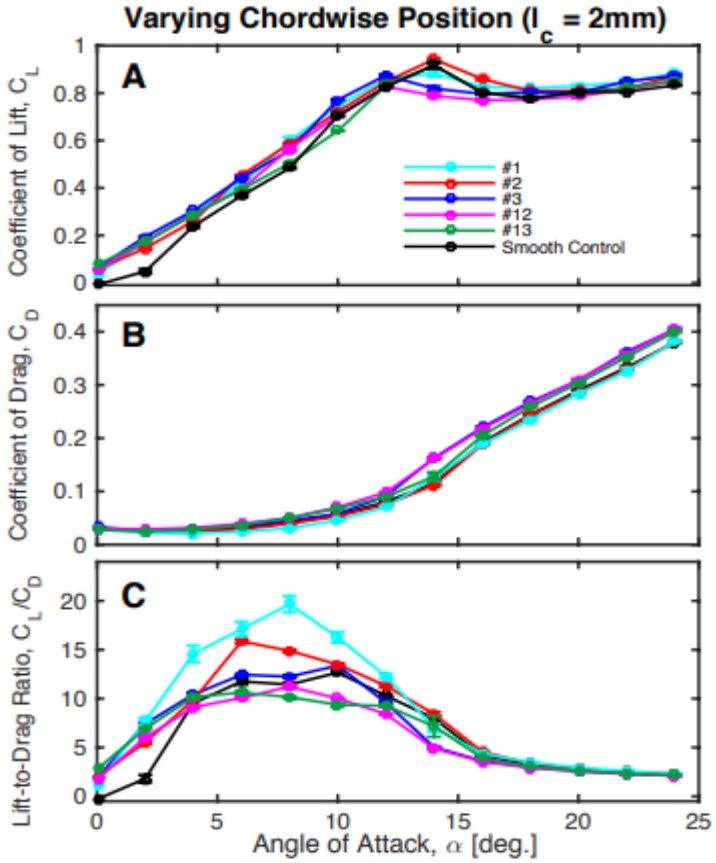

Result of Foils #1, #2, #3, #12 and #13

VARYING TILT ANGLE OF DENTICLES

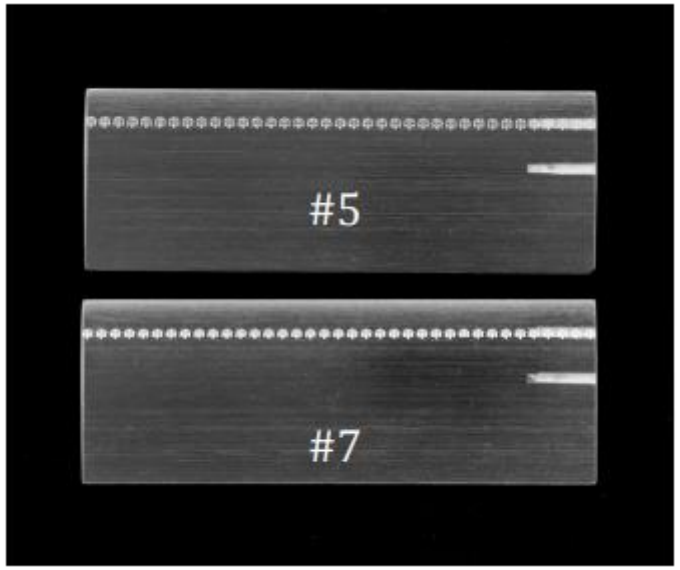

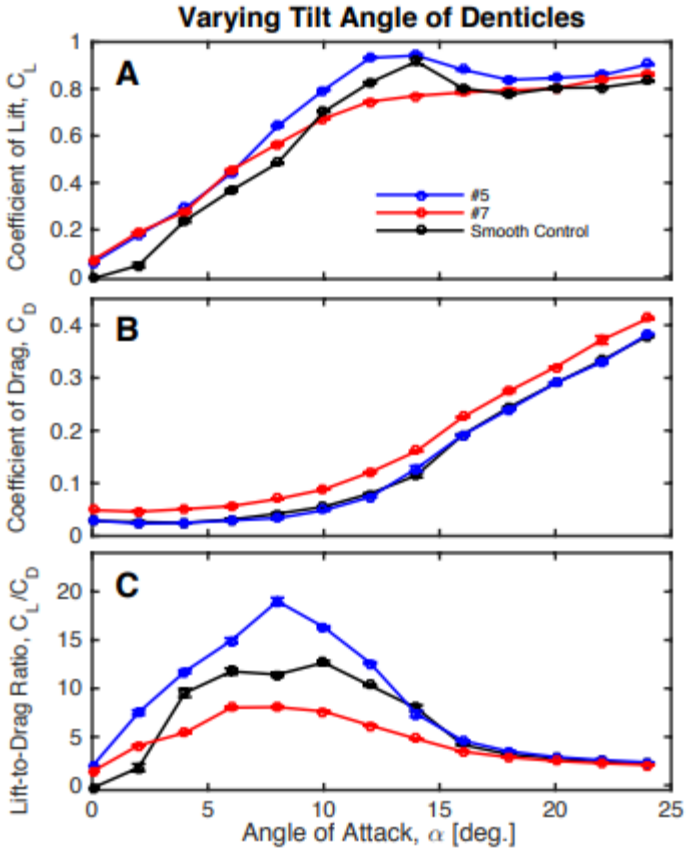

Result of Foils #5, #7

VARYING SPANWISE SEPARATION OF DENTICLES

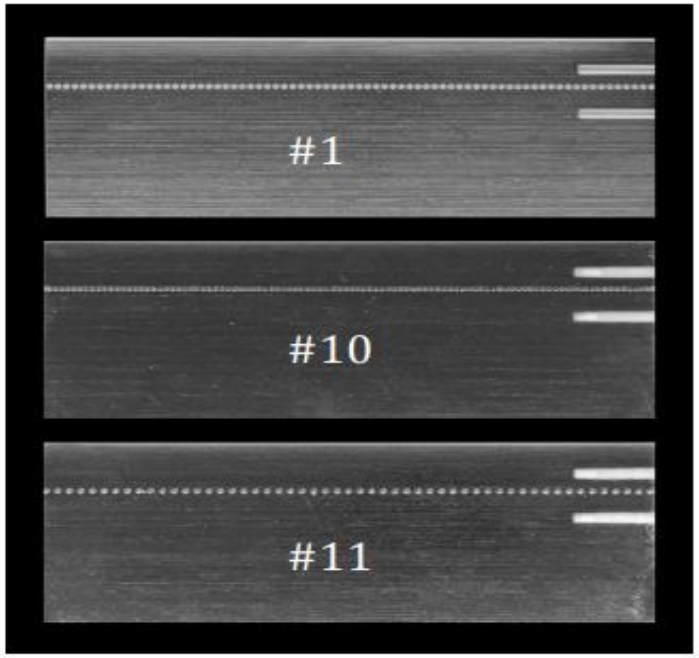

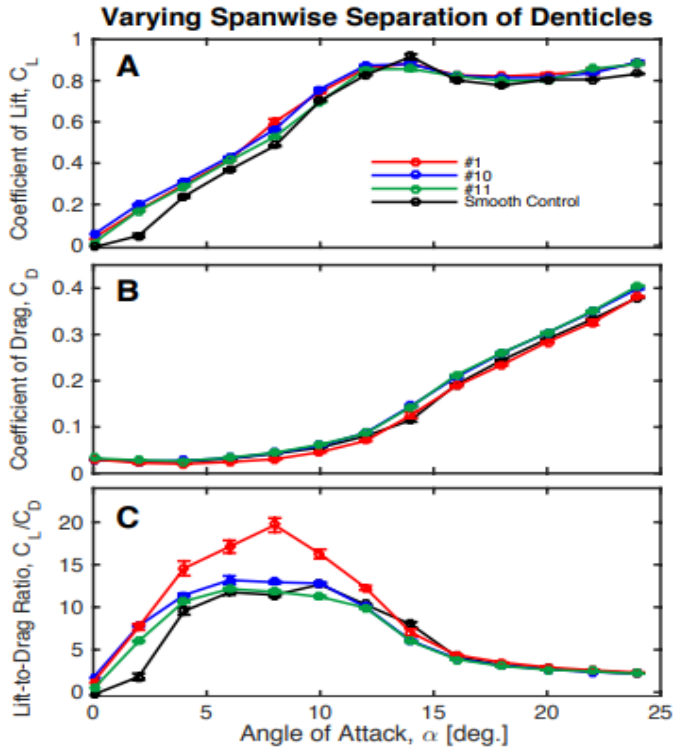

Result of Foils #1, #10 and #11

VARYING CHORDWISE SEPARATION WITH TWO ROWS OF DENTICLES

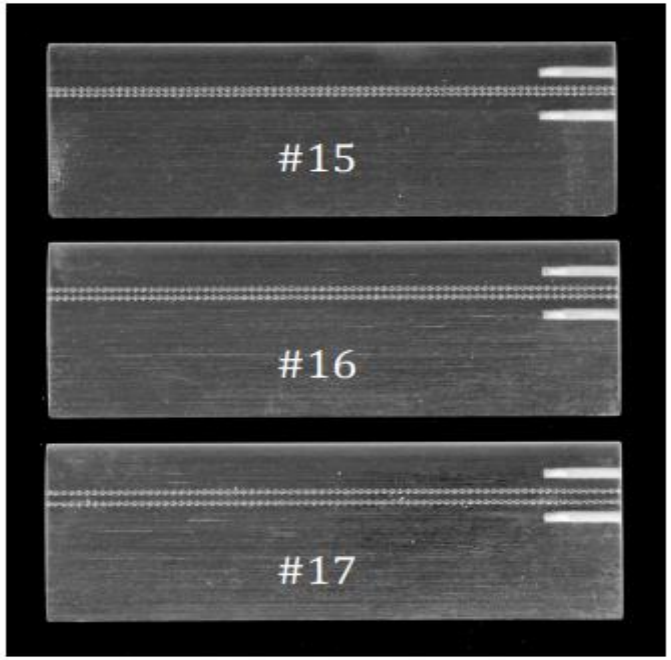

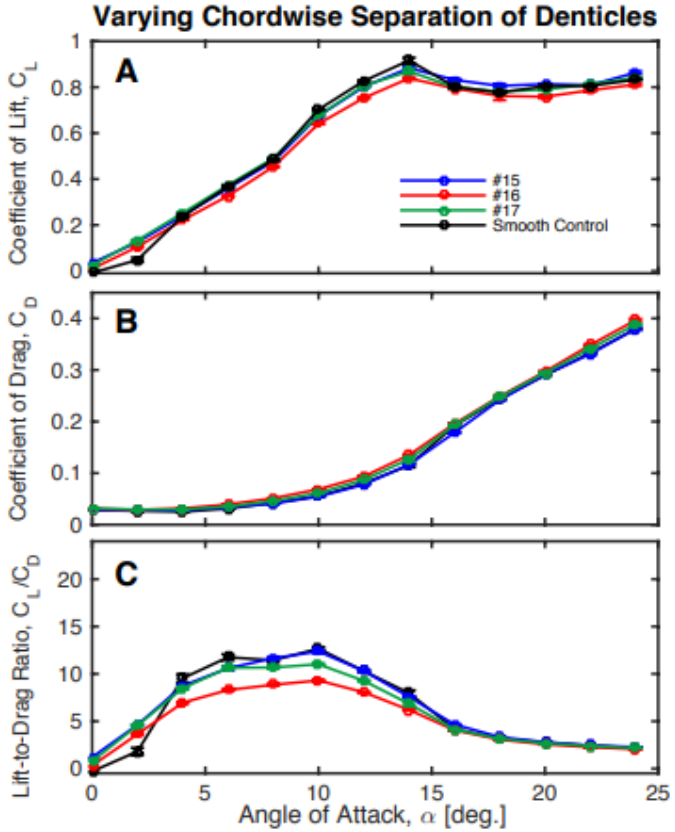

Result of Foils #15, #16 and #17

VARYING PATTERN WITH TWO ROWS OF DENTICLES

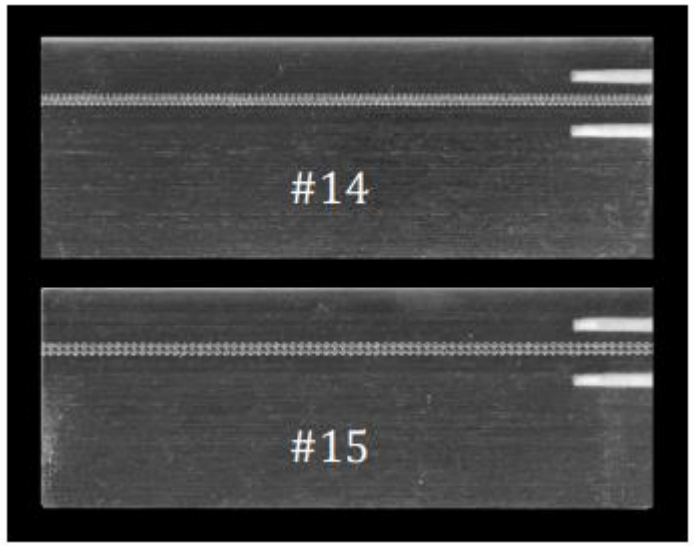

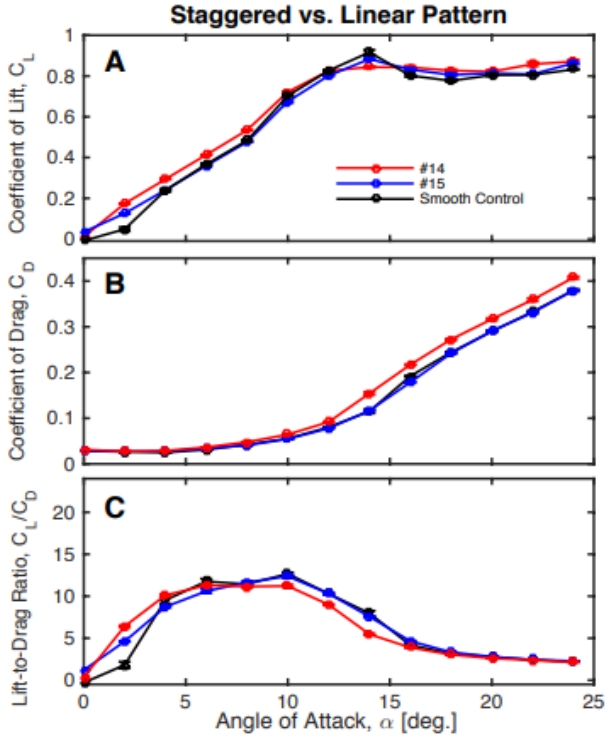

Result of Foils #14, #15

FOILS WITH 4 OR MORE ROWS OF DENTICLES

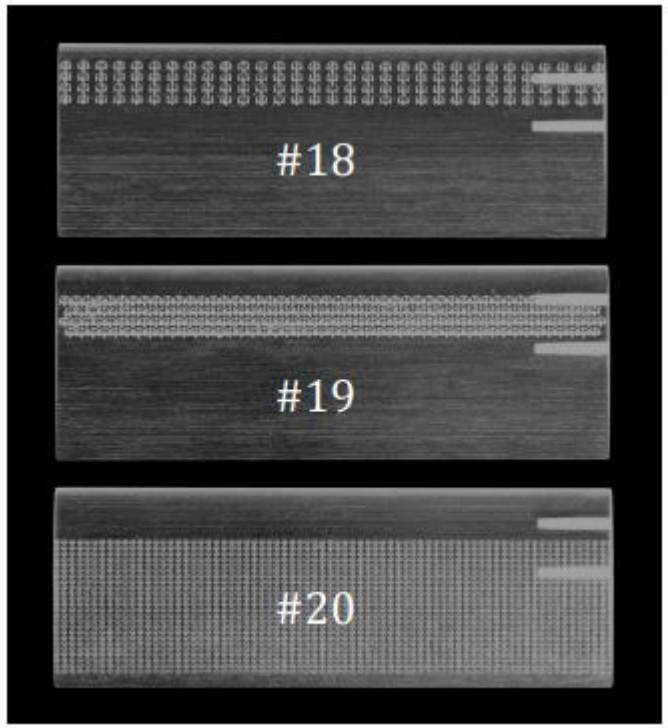

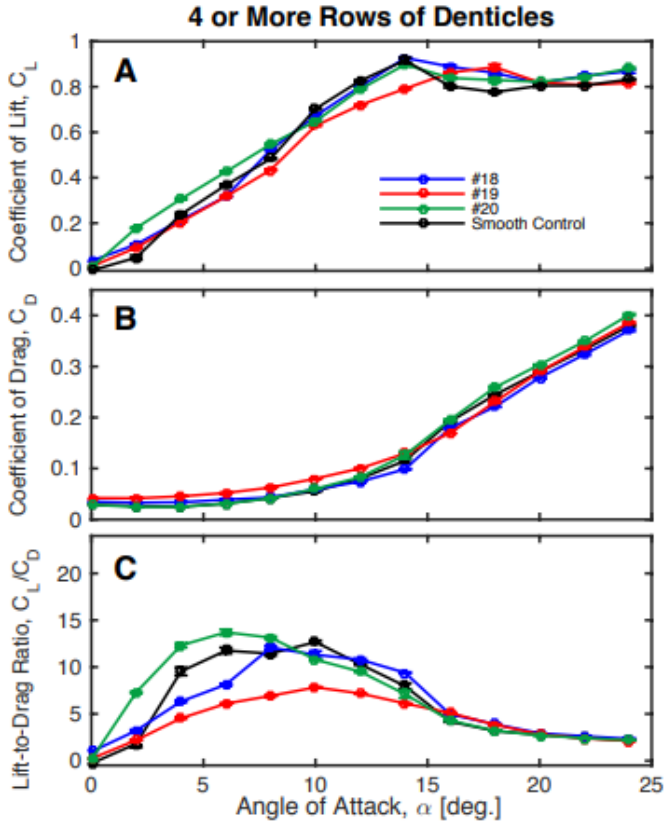

Result of Foils #18, #19 and #20

RESULT & DISCUSSION

- Experimental results for the best shark denticle aerofoil. Evolution of (a) lift coefficient, (b) drag coefficient. (c) lift-to-drag ratio as a function of the angle of attack. In all plots, the results for the best shark denticle foil (red lines) are compared to those for the corresponding smooth control (black lines).

- Each data point is based on nine total tests and standard error bars are included (note that most error bars are small enough to be contained within the data marker). The inset in (b) is a schematic depicting the angle of attack (α) of the aerofoil (x being the direction of fluid flow and y being the direction of lift).

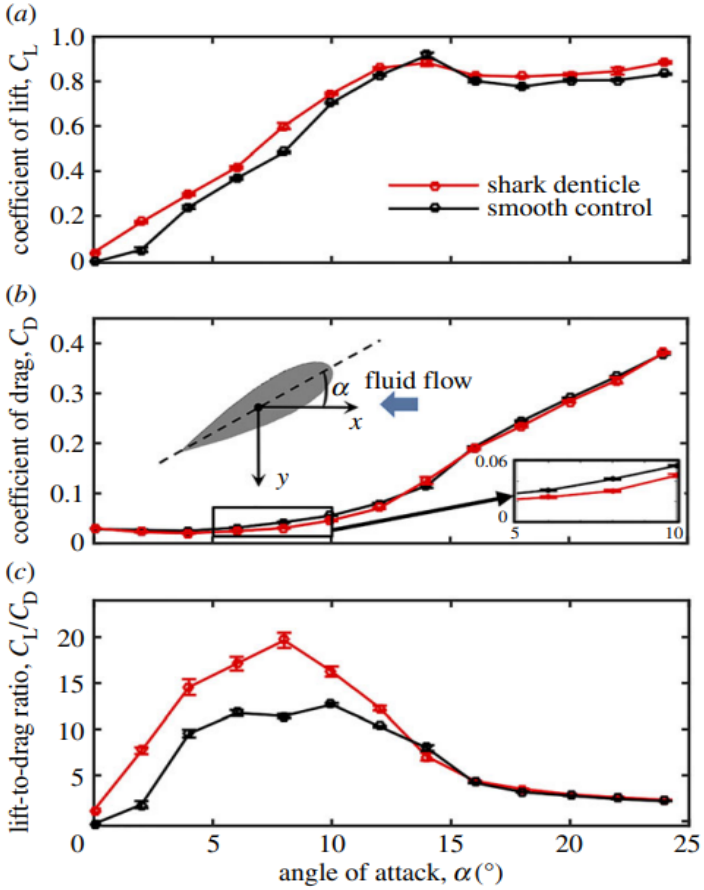

Flow response shark denticle vs smooth control

- While most foils behaved roughly similar to the denticle-free control, a few of them exhibited significantly enhanced performance We report results of the experiments for the best performing foil, which comprises a single row of denticles.

- Each of which covers a footprint of roughly 2 mm by 2 mm and has a middle-ridge height of 0.7 mm placed at 26% along the chord and with a spanwise separation of 1 mm. Note that the 26% chordwise placement is consistent with previous work on NACA0012 aerofoils, which has shown that the minimum pressure happens right after this location, making the flow susceptible to separation.

- The results show for the best shark denticle foil exhibit three key features. First, we observe an increase in lift at almost all angles of attack for the foil with shark denticles compared to the corresponding smooth control (i.e., CL shark / CL control = 3.55, 1.24, 1.13, 1.24, 1.06, 1.04, 0.96, 1.03,1.06 at α = 2°, 4°, 6°, 8°, 10°, 12°, 14°, 16°, 18°, respectively.
- We even find that positive lift is generated at zero angle of attack for the shark denticle foil (CL shark = 0.04 at α = 0°), whereas, as expected, we see no lift being generated by the smooth, symmetric control foil for α = 0°.
- Second, the aerofoil with shark denticles reduces drag compared to the smooth control at almost all angles of attack smaller than the angle at which stall occurs (CD shark/CD Control = 1.06, 0.84, 0.81, 0.78, 0.72, 0.83, 0.87 at α = 0°, 2°, 4°, 6°, 8°, 10°, 12°, respectively. with drag reduction comparable to previously designed synthetic shark skin surfaces.
- Third, because of the two combined effects described above, we observe substantial enhancements in the lift-to-drag ratio (CL/D = CL / CD). More specifically, we find that CL/D shark / CL/D control = 4.23, 1.53, 1.46, 1.72, 1.28 and 1.19 at α = 2°, 4°, 6°, 8°, 10° and 12°, respectively.

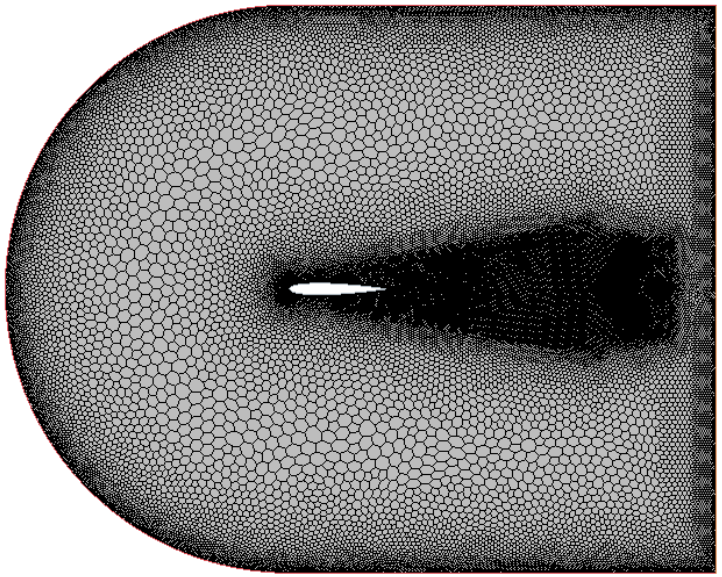

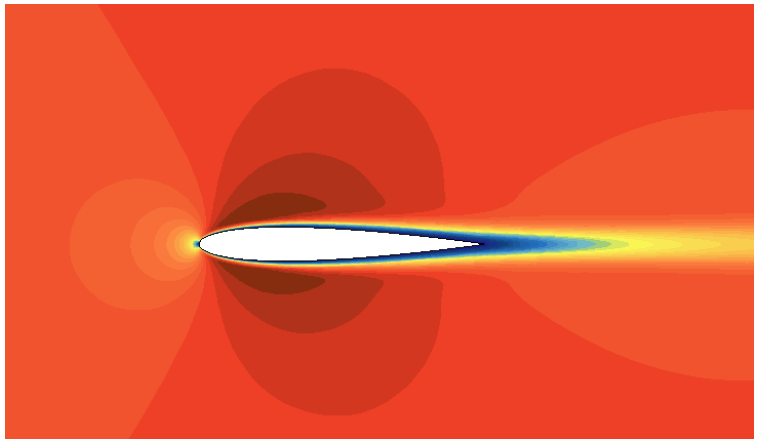

Advance Approach

AIRFOIL WITH 2D BUMP PROFILE

- To further understand the effect of the denticles on the aerodynamic performance of the aerofoils, first we focused on the robust lift enhancement at low angles of attack. Guided by a previous numerical study that demonstrated that a simple 2D bump arranged on a flat plane can generate a negative pressure coefficient. We constructed a foil in which the row of denticles was replaced with a simple 2D bump profile (with non-zero curvature only in the chordwise direction).
- This bump was arranged in the same chordwise location and had height and leading-edge curvature that matches those of the shark denticles (see figure for details on the morphology of this aerofoil). Furthermore, the bump had a streamlined design on its downstream side to reduce its generated pressure drag.
- Comparison between the profile of the 2D bump (red line) and the representative model of the shark denticle. (B) Side view of the 2D bump. (C) Chordwise placement of the 2D bump on the foil (d/L=0.26). (D) Isometric view of the 2D bump foil.

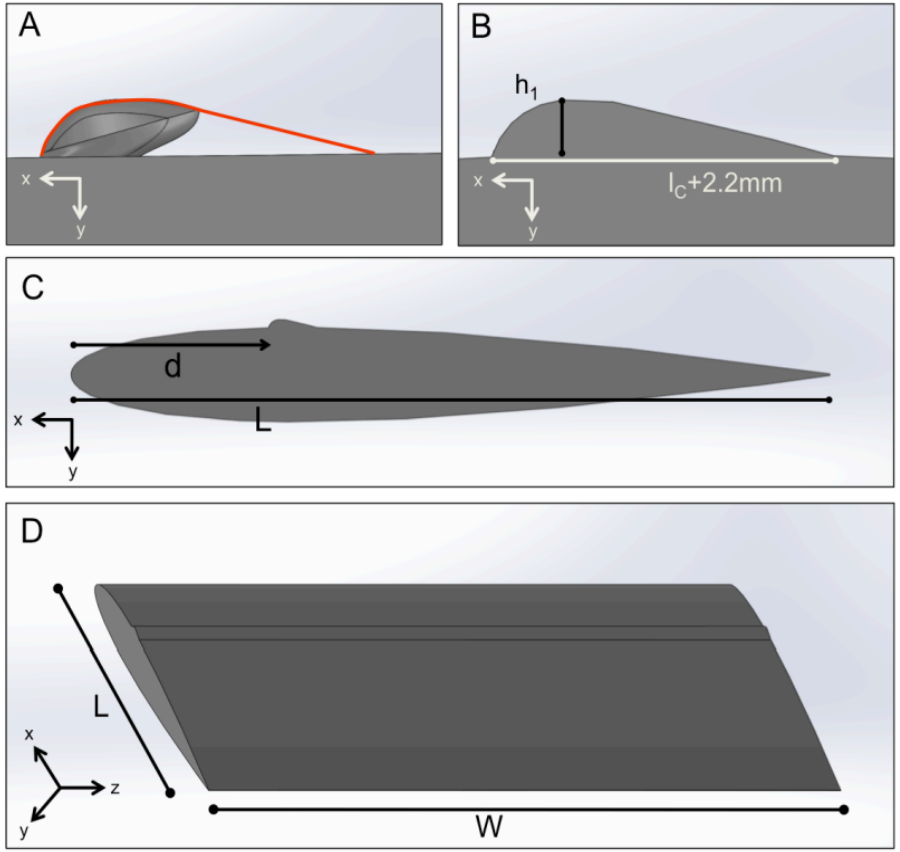

- Above shows the morphology of the 2D bump foil. The leading-edge curvature matches the shark denticle middle ridge leading edge curvature. However, rather than having an overhang like the shark denticle does, the bump attaches to the foil downstream from where the shark denticle middle ridge ends.

- This gives the 2D bump a streamlined nature so as to reduce pressure drag. Note that all parameters and dimensions (h1, IS, d, L, W) shown match exactly that of the best shark denticle foil (Foil #1). Specifically, h1=0.7mm, IC=2mm, d/L=0.26, L=68mm and W/L=2.8.

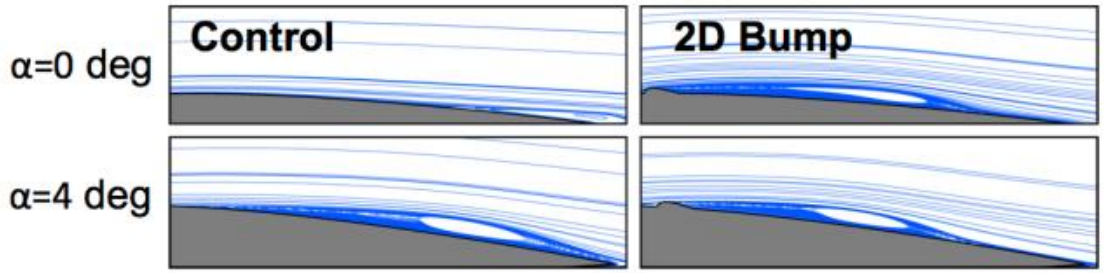

- The experimental lift, drag and lift-to-drag ratio for this 2D bump profile on a foil are presented. If we look specifically at the lift coefficient reported in figure 24a, we see that this simple 2D bump profile enhances lift at low angles of attack (CL 2Dbump / CL control = 3.08 and 1.17 at $\alpha = 2^\circ$ and $\alpha = 4^\circ$, respectively) and generates non-zero lift at $\alpha = 0^\circ$ (CL 2Dbump = 0.09 at $\alpha = 0^\circ$).

- Interestingly, while at $\alpha = 2^\circ$ and $\alpha = 4^\circ$, the foil with the 2D bump profile generates close to the same amount of lift as the one with the shark denticles (CL 2Dbump / CL shark = 0.87 and 0.94 at $\alpha = 2^\circ$ and 4°, respectively), it results in over twice the amount of lift at zero angle of attack (CL 2Dbump / CL shark = 2.41 at $\alpha = 0^\circ$). These results confirm that the complex shape of the shark denticles arranged on the foil is not necessarily crucial to achieve lift enhancement at low angles of attack, and suggests that a continuous chordwise curved profile can further enhance CL.

- However, the results reported also demonstrate that the foil with the simple 2D bump profile loses its lift benefits relative to the control at higher angles of attack unlike the shark denticle foil (CL 2Dbumb / CL control = 0.88, 0.95, 0.91 at α = 10°, 12°, 14°, respectively). At these angles right before and at stall, it is actually producing less lift than the control. Moreover, we also note that the 2D bump profile does not alter the drag greatly compared to the smooth control (except at α = 10° and 12°)
- Because of the last two effects, and when compared with the best denticle-containing foil, we find that the 2D bump profile exhibits a significantly lower lift-to-drag ratio across nearly all measured angles of attack. Experimental results for the 2D bump profile on an aerofoil. Evolution of (a) lift coefficient, (b) drag coefficient and (c) lift-to-drag ratio as a function of the angle of attack.
- In all of the plots, the results for the 2D bump profile on an aerofoil (blue lines) are compared to those for the corresponding smooth control (black lines). Each data point is based on nine total tests and standard error bars are included (note that most error bars are small enough to be contained within the data marker). The inset in (b) depicts the morphology of the 2D bump profile.

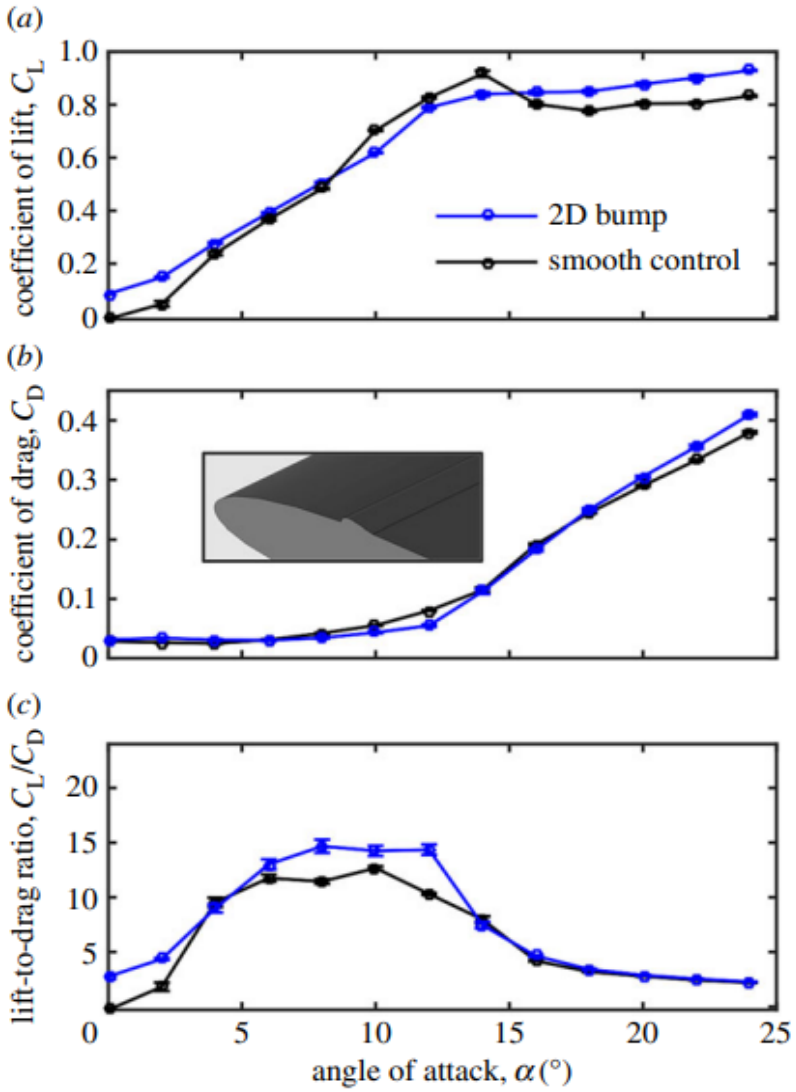

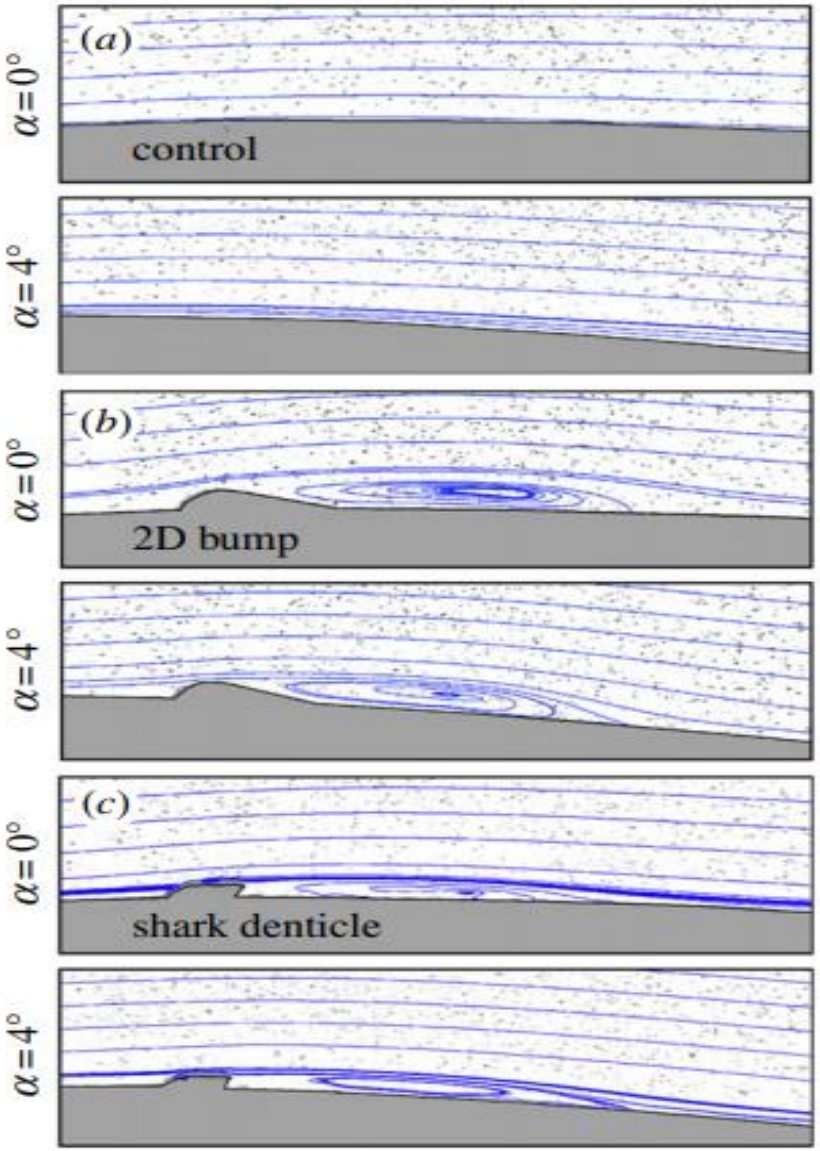

- Flow streamlines obtained via particle image velocimetry (PIV). PIV streamlines for the (a) smooth, (b) 2D bump profile and (c) shark denticle foils are shown at $\alpha = 0^\circ$ and 4°, angles at which lift is being significantly enhanced by the 2D bump profile and shark denticle foils. A short separation bubble develops behind both the shark denticle and 2D bump foils, helping to provide further suction and therefore lift for these foils compared to the control.
- Because of the geometric simplicity of the 2D bump foil compared to the shark denticle foil, 2D simulations of this system were conducted. As done with the experiments, CFD data were computed for angles of attack that extended past stall. For the CFD, we observe similar results to those seen in the experiments.
- Positive lift is being generated at zero angle of attack by the 2D bump profile ($C_L = 0.22$), and we calculate a 946% and 11% increase in lift generated at $\alpha=2^\circ$ and $\alpha=4^\circ$ respectively compared to the control. In addition, we notice that lift enhancements by the 2D bump foil are lost at higher angles of attack just as was the case in experiments.

- At low angles of attack, a separation bubble is formed by the 2D bump profile, which leads to separation, and which in turn likely ultimately degrades the performance of the 2D bump foil at higher angles. In regards to drag, it is important to note that at zero angle of attack a very similar drag coefficient is seen in CFD compared to the experiments (both just a bit below 0.03).
- Because of this lift and drag results, we see an overall qualitatively similar L/D curve as was seen in experiments. The CFD streamlines for the 2D bump and control for two low angles of attack at which lift is being enhanced by the 2D bump profile ($\alpha=0^\circ$ and $\alpha=4^\circ$). Analyzing these images, we see that at 0° a short separation bubble is being generated by the 2D bump foil yet not in the smooth control (as was the case with the shark denticle foil).
- At 4° we do see a separation bubble developing at the trailing edge of the smooth control. However, this separation bubble is fairly large and does not quite reattach at the trailing edge of the foil, negatively affecting lift. In the 2D bump foil, we see the separation bubble in both CFD and PIV at $\alpha=4^\circ$ much further upstream, which is a more beneficial location in regards to the pressure gradient along the chord as previously discussed. We should note, however, that there are some differences in the experimental and CFD results, such as the angle at which each of the foils stall and the maximum lift and drag being generated.
- The 2D CFD calculations here are inherently somewhat different than the 3D experiments which include three-dimensional effects; CFD is a much more idealized version of the experiments. In the experiments, for example, tip vortices may reduce the size of the separation bubble. In spite of some inherent differences between the two, we have shown that there are qualitative similarities between the CFD and experiments, including the following: (i) a positive lift enhancement at low angles of attack, (ii) non-zero lift at zero angle of attack

- iii) the loss of lift increases relative to the control near and at stall. Furthermore, similar flow mechanisms are seen in both the CFD and PIV streamlines, where short separation bubbles form downstream from the trailing edge of the 2D bump profile. Computational fluid dynamic (CFD) results. Evolution of (A) lift coefficient, (B) drag coefficient and (C) lift-to-drag ratio as a function of the angle of attack. (D) Numerical snapshots showing the streamlines for the control and 2D bump at $\alpha = 0^\circ$ and 4°. The reason behind the lift benefit at low angles of attack seen by both the shark denticle and 2D bump profile in comparison to the control can be further understood by inspecting the flow streamlines obtained via PIV.

- The streamlines at $\alpha = 0^\circ$ and 4° reveal that, in the presence of both the shark denticles and the 2D bump profile, a short separation bubble forms behind their trailing edge. While typically separation bubbles are thought to negatively affect the performance of an aerofoil [8,10], it has also been shown that short separation bubbles (that fully reattach to the aerofoil) can help to maintain a higher level of suction a bit further down the chord of the aerofoil, providing a region over which the pressure distribution along the chord plateaus rather than dropping off further.

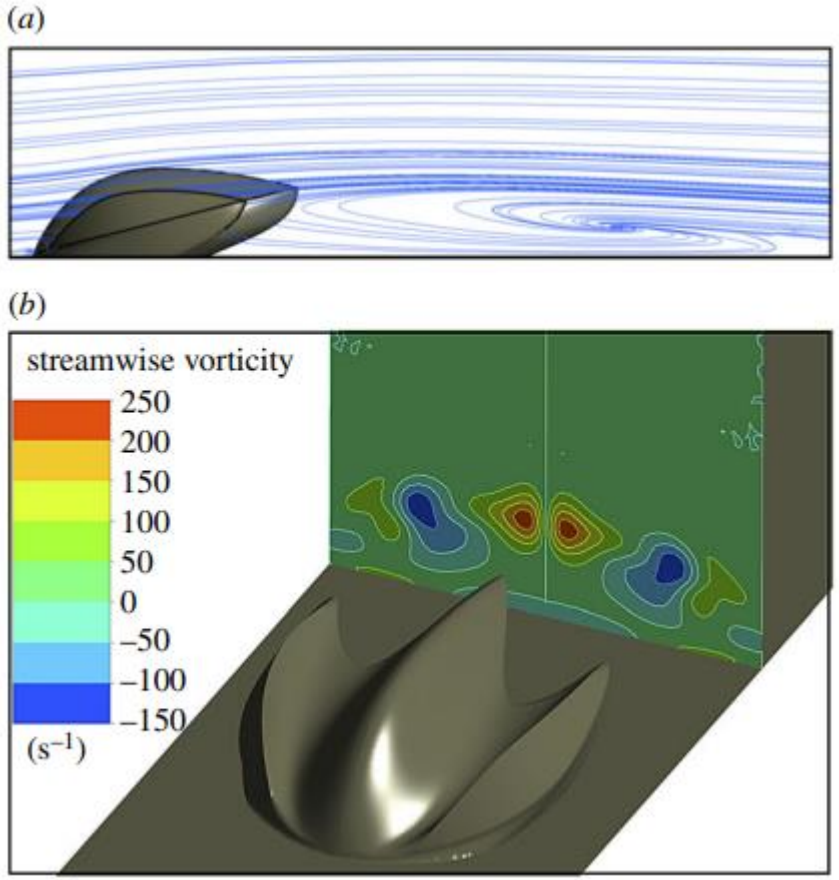

- These streamwise vortices are likely responsible for drag reduction and also likely help to maintain lift at higher angles of attack by bringing higher momentum fluid from the outer part of the boundary closer to the wall and thus help replenish the momentum in the boundary layer which would have been lost to skin friction. It is further known that the interaction among these vortices is crucial in determining their aerodynamic advantages [33,34]. For instance, placing the vortex generators too close to each other in the spanwise direction can lead to destructive interference of the streamwise vortices, which ultimately reduces the performance of the aerofoil.

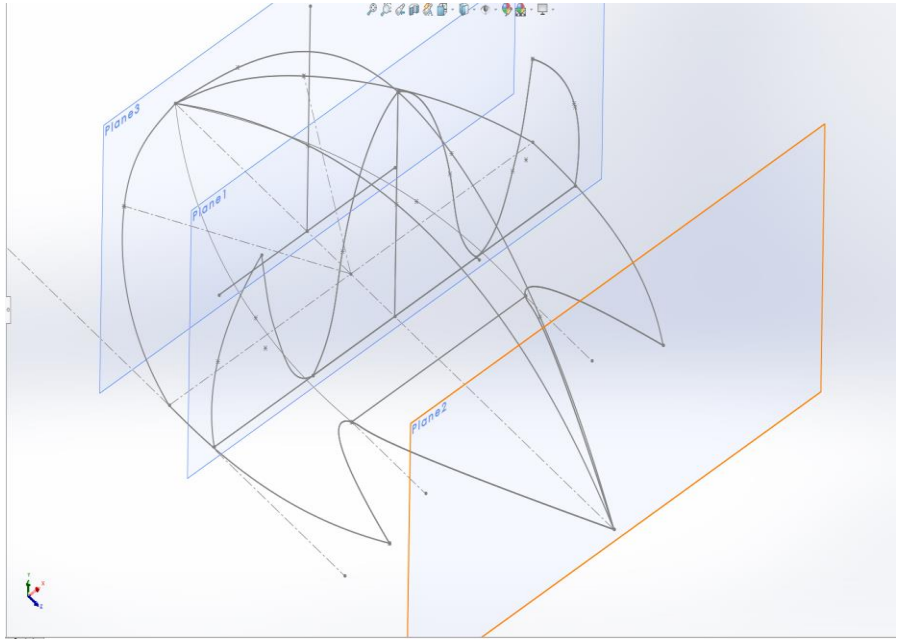

- This observation helps explain the high sensitivity of the drag coefficient to the morphology and placement of the denticles that we found in our experiments. CFD analyses of a shark denticle model on a flat plate. (a) Numerical snapshot showing the flow streamlines. Our analyses predict the formation of a short separation bubble in the wake of the denticle (b) Contours of the streamwise vorticity (the rate at which the streamwise-moving fluid is rotating just after the denticle) on a plane perpendicular to the flow just downstream from the denticle. The separation bubble and streamwise vortices shown in (a) and (b) help to enhance lift and reduce drag when the shark denticle is correctly placed on an aerofoil.

AIRFOIL WITH CONTINUOUS SHARK-INSPIRED PROFILE

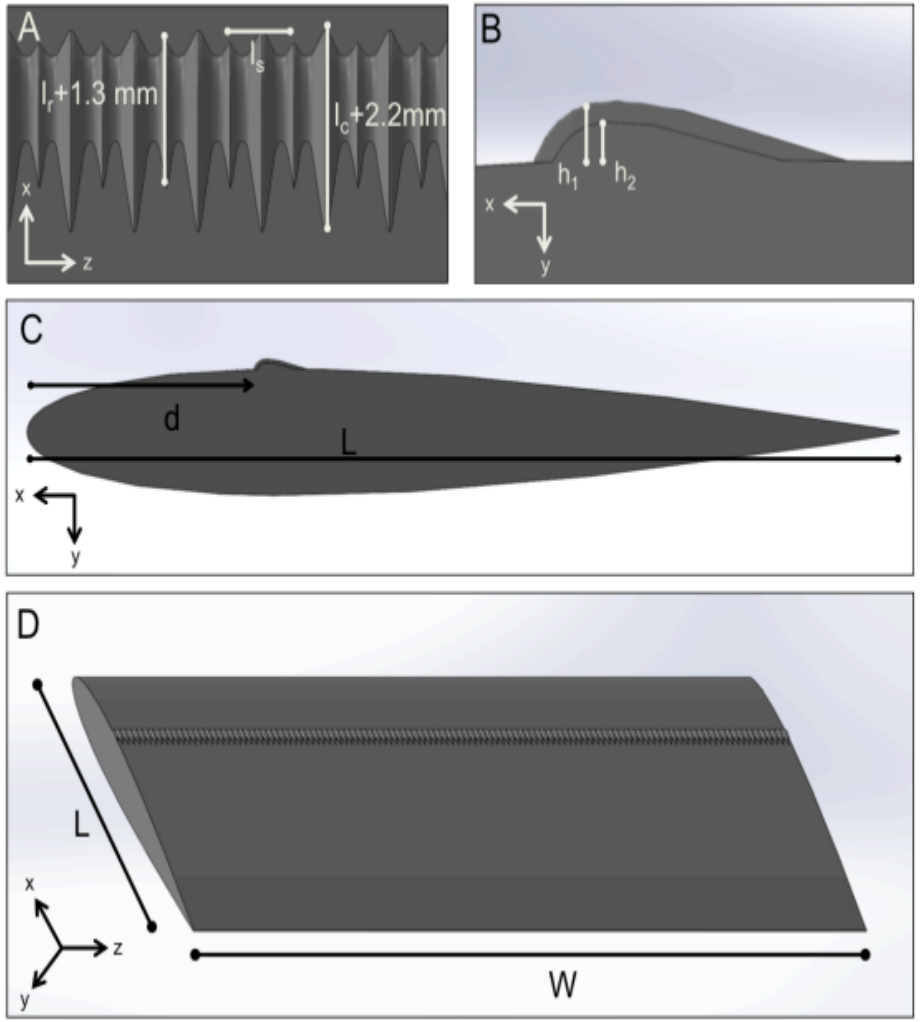

- Guided by all these results, we then tried to improve the aerodynamic performance of the aerofoil by designing a geometric perturbation that takes advantage of the multiple mechanisms that were seen to be beneficial in the foils with the shark denticles and the 2D bump. More specifically, we designed a geometric perturbation that combines the ridges of the shark denticle with the continuous chordwise curved profile of the 2D bump to achieve the lift-to-drag ratio benefits of the shark denticle.

- While yet also improving the lift further at very low angles of attack (especially $\alpha = 0°$) in the way seen by the 2D bump profile. While this new morphology's chordwise cross-section is designed similarly to that of the 2D bump, its spanwise curvature and morphology resembles that of the denticle except for the fact that it has a continuous sinusoidal-like nature as opposed to the finite nature of the shark denticles placed side-by-side on an aerofoil. We refer to this new continuous streamlined morphology as the 'continuous shark-inspired profile'. we show top, side, and isometric views of the continuous shark-inspired profile. Essentially, this morphology can be thought of as one continuous shark denticle that runs the full span of the foil at a chordwise placement of $d/L = 0.26$.

- The leading edge chordwise curvature matches that of the shark denticle (just like the 2D bump profile did). This morphology also has an extremely similar structure as that of the denticle with a long chordwise middle ridge between two smaller side ridges. The side ridges have been extended an extra 1.3mm and the middle ridge an extra 2.2mm so as to give this profile a very streamlined extended shape like that of the 2D bump profile, yet with pronounced chordwise ridges like that of the denticle).
- Similarly to foil #1, h1 =0.7mm, h2 =0.5mm, IS =1.5mm, IC =2mm, IR =1.6mm, d/L=0.26, L=68mm, W/L=2.8. (A) Top and (B) side views of the continuous shark-inspired profile. (C) Chordwise placement of the profile on the foil (d/L=0.26). (D) Isometric view of the continuous shark-inspired foil. we report the experimental results for the aerodynamic response of an aerofoil with this continuous shark-inspired profile placed at 26% along the chord.
- First, focusing on lift at low angles of attack, we find that this aerofoil generates roughly the same amount of lift as the one with the 2D bump profile, and over twice that of the one with shark denticles at $\alpha = 0^\circ$ (CL cont / CL 2Dbump = 1.03 and CL cont / CL shark = 2.47).We also see that the foil with this continuous shark-inspired profile results in coefficients of lift similar to those seen for the cases of the 2D bump profile and shark denticles at other low angles of attack (CL cont / CL 2Dbump = 1.19, 1.09 and CL cont / CL shark = 1.04, 1.03 at $\alpha = 2^\circ$ and 4°, respectively).

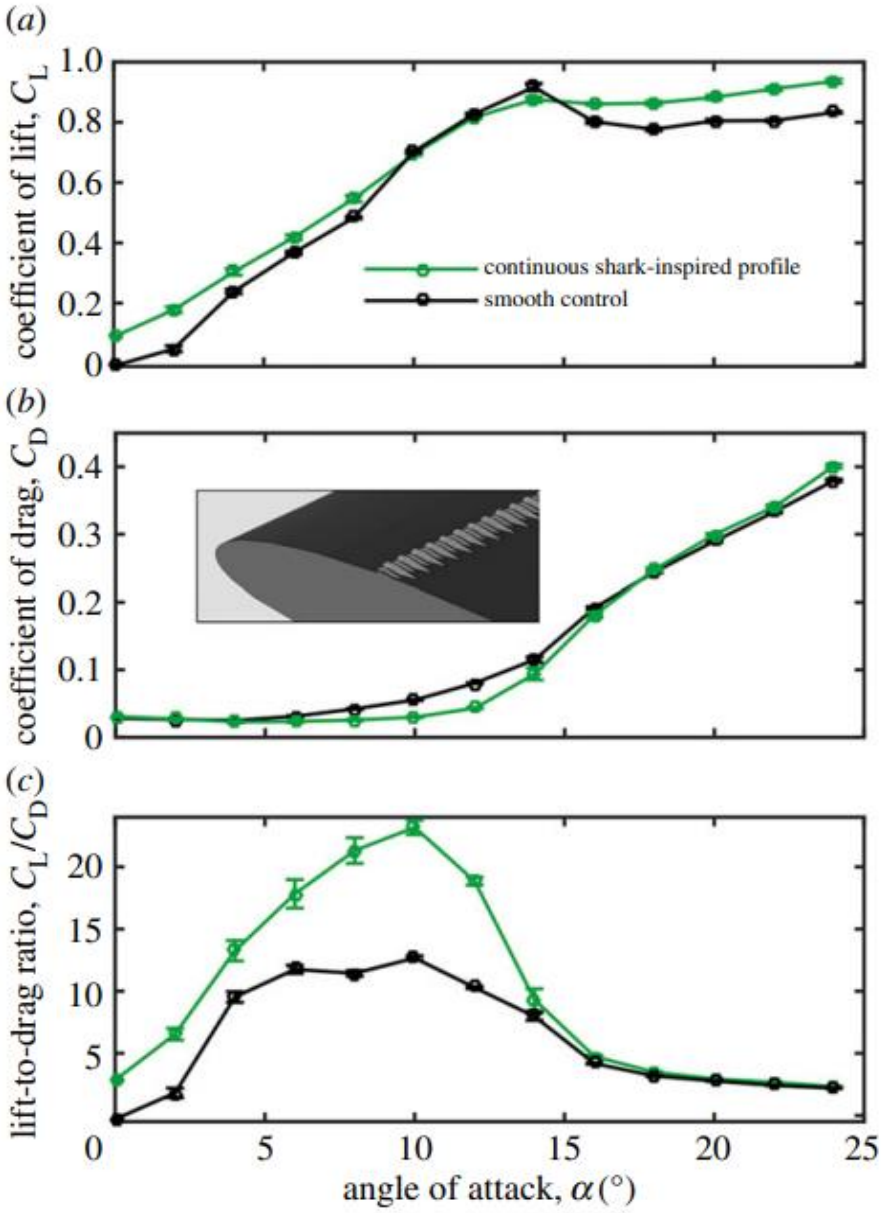

- Second, our results indicate that this continuous shark inspired profile does not lose these lift benefits as much at higher angles of attack prior to stall. Third, we find that the continuous shark-inspired profile leads to even more drag reduction than the shark denticles (figure 30b). This is especially evident at angles of attack just before stall, with CD cont / CD control = 0.54 and 0.53 at $\alpha = 10^{\circ}$ and 12°, respectively (resulting in CD cont / CD shark = 0.65 and 0.62 at $\alpha = 10^{\circ}$ and 12°, respectively).
- This may in part be helped by the streamlined nature of the continuous shark-inspired profile. Finally, it is important to note that the observed high lift and low drag lead to large lift-to-drag ratio increases (CL/D cont / CL/D control = 3.61, 1.39, 1.52, 1.86, 1.83 and 1.83 at $\alpha = 2^{\circ}$,4°, 6°, 8°, 10° and 12°, respectively - see figure 30c). Experimental results for the aerofoil with a continuous shark inspired profile. Evolution of (a) lift coefficient, (b) drag coefficient and (c) lift-to-drag ratio as a function of the angle of attack.
- In all plots, the results for the continuous shark-inspired profile (green lines) are compared to those for the corresponding smooth control (black lines). Each data point is based on nine total tests and standard error bars are included (note that most error bars are small enough to be contained within the data marker). Specifically, we see from (which shows a comparison of the lift-to-drag ratio improvements of all three main foils discussed) that the continuous shark-inspired profile outperforms the 2D bump profile at all angles of attack and the shark denticle at just about all angles of attack.
- This is because the continuous shark-inspired profile is able to produce the same lift benefits as the 2D bump at low angles of attack (especially $\alpha = 0^{\circ}$) without losing these lift benefits as much at higher angles of attack (like the 2D bump does), in addition to greatly reducing drag at higher angles (like the shark denticle is able to). Note that in we also indicate with a filled in marker the angle at which the maximum lift-to-drag ratio occurs for each foil. Again, we find that the continuous shark inspired profile produces the greatest improvement at this angle.

COMPARISON OF THE RESULTS FOR THE FOILS DISCUSSED

- First, all three foils provide great improvements in L/D at low angles of attack (i.e. at $\alpha = 2^\circ$), with the shark denticle and continuous shark-inspired profile foils performing significantly better. This is because, although the 2D bump profile enhances lift over twice that of the shark denticle at $\alpha=0^\circ$, it loses a lot of those lift benefits at higher angles of attack and does not produce a lot of drag reduction since it is not a vortex generator.

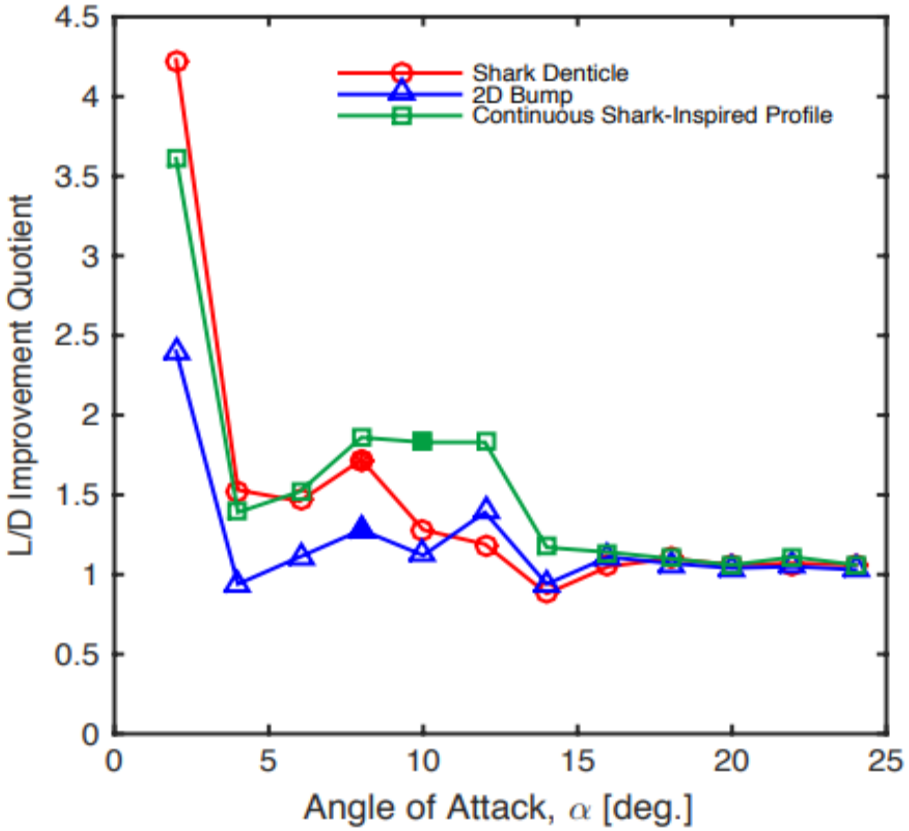

- Second, the continuous shark-inspired profile is outperforming the other two foils at the majority of angles of attack. This is because this profile, which combines aspects of the 2D bump profile and the shark denticle, is able to produce the same lift benefits as the 2D bump at $\alpha = 0^\circ$ without losing these lift benefits as much at higher angles of attack (like the 2D bump does), in addition to greatly reducing drag at these higher angles. we also indicate with a filled in marker the angle at which the max L/D occurs for each foil. Note that at this angle the foil can move with its most advantageous lift-to-drag ratio.

- So for example, if a given application does not have a mandatory angle of attack at which it must move, then this angle of attack would be the most advantageous to use for generating a lot of lift without producing too much drag. We see from that, like in the case of most angles of attack, the continuous shark-inspired profile produces the greatest improvements at this max L/D (as seen by comparing the filled in markers for each foil).

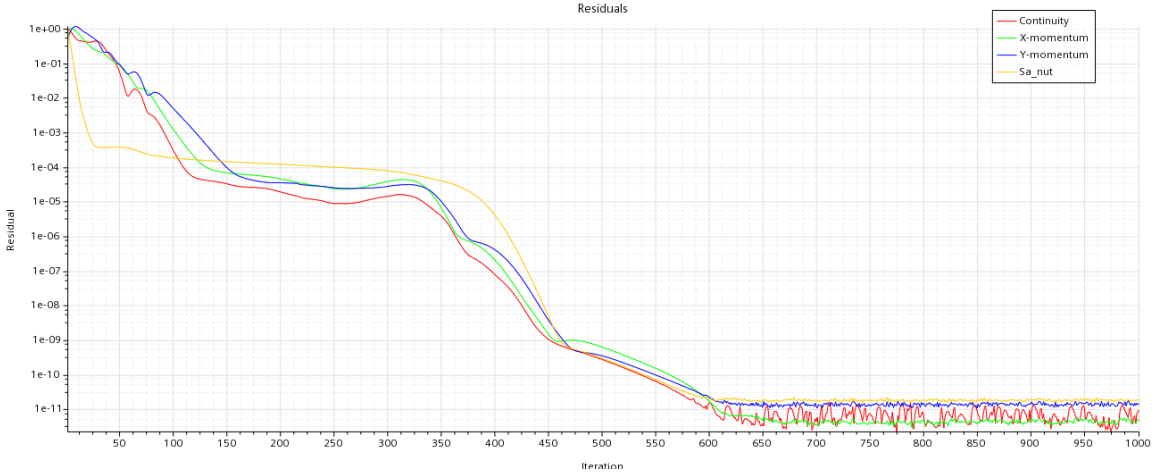

- In addition to these great lift-to-drag ratio improvements, this continuous shark-inspired profile has another important advantage over the other foils discussed here. Although there has been increased interest in recent years aimed at reproducing the hydrodynamic performance of shark denticles for use on engineered surfaces, one major obstacle to the mass production of these shark skin-inspired geometries has been the structural complexity of the denticles.

- While it has been demonstrated previously that it is possible to replicate these forms through the use of 3D printing, this approach is unfortunately not scalable, and the undercuts and overhangs present on the native denticles prevent the direct moulding of these specific geometries using conventional manufacturing strategies. The continuous shark inspired profile described here circumvents these problems and is easily amendable to roll-to-roll embossed fabrication, bringing this technology one step closer to large-scale adoption for aquatic and aerospace applications.

Conclusion

- In this study, we have taken inspiration from shark denticles to design a set of profiles that significantly improve the aerodynamics of aerofoils. In contrast to previous studies on shark skin that have mostly focused on drag reduction/ thrust improvement, we showed that the denticles also generate lift, resulting in high lift-to-drag ratio improvements.
- Specifically, we found comparable results to those of the best previously reported low-profile vortex generators at higher angles of attack near stall, and even much higher improvements at low angles of attack ($\alpha < 4°$). The remarkable results shown here were achieved by using two mechanisms. First, the shark-inspired profiles trip the boundary layer and generate a short (reattaching) separation bubble that provides extra suction along the chord and thereby enhances lift.
- Second, the spanwise curvature of the denticles helps to generate streamwise vortices that can lead to drag reduction and prevent lift losses at higher angles of attack. While in this study we have considered the ideal case of the denticles' ridges perfectly parallel to the flow, future work will investigate how sensitive the aerodynamic response of the aerofoils is to the orientation of the denticles with respect to the flow.
- Finally, the results discussed here may have implications for understanding the function of shark denticle morphology. Shark skin denticles have been shown to alter the position and strength of the leading edge vortex in experimental studies, and it is likely that the lift effects observed here contribute to a thrust enhancement effect of shark skin resulting in increased self-propelled swimming speeds.

Reference

- Raymer D. 2012 Aircraft design: a conceptual approach, 5th edn. New York, NY: AIAA.
- Amitay M, Smith B, Glezer A. 1998 Aerodynamic flow control using synthetic jet technology. In 36th AIAA Aerospace Sciences Meeting and Exhibit, Reno, NV, 12 January. Reston, VA: AIAA.
- Kiedaisch J, Nagib H, Demanett B. 2006 Active flow control applied to high-lift airfoils utilizing simple flaps. In 3rd AIAA Flow Control Conference, San Francisco, CA, 5 June. Reston, VA: AIAA.
- Pack L, Schaeffler N, Yao C, Seifert A. 2002 Active control of flow separation from the slat shoulder of a supercritical airfoil. In 1st Flow Control Conf.,St Louis, MO, 26 June. New York, NY: AIAA.
- Kiedaisch J, Demanett B, Reinhard P, Nagib H. 2007 Active flow control for high lift airfoils: dynamic flap actuation. In 45th AIAA Aerospace Sciences Meeting and Exhibit, Reno, NV, 10 January. Reston, VA: AIAA.
- Amitay M, Parekh DE, Smith DR, Kibens V, Glezer A. 2001 Aerodynamic flow control over an unconventional airfoil using synthetic jet actuators. AIAA J. 39, 361– 370. (doi:10.2514/2.1323)
- Lin JC, Howard FG, Selby GV. 1990 Small submerged vortex generators for turbulent flow separation control. J. Spacecr. Rockets 27, 503– 507. (doi:10.2514/3.26172)
- Lin JC. 2002 Review of research on low-profile vortex generators to control boundary-layer separation. Prog. Aerosp. Sci. 38, 389– 420. (doi:10.1016/S0376-0421(02)00010-6

- Yao C, Lin J, Allen B. 2002 Flowfield measurement of device-induced embedded streamwise vortex on a flat plate. In 1st Flow Control Conference. Reston, VA:American Institute of Aeronautics and Astronautics.
- Kerho M, Hutcherson S, Blackwelder RF, Liebeck RH.1993 Vortex generators used to control laminar separation bubbles. J. Aircr. 30, 315 – 319. (doi:10.2514/3.46336)
- Lin JC, Robinson SK, McGhee RJ, Valarezo WO. 1994 Separation control on high-lift airfoils via microvortex generators. J. Aircr. 31, 1317– 1323. (doi:10.2514/3.46653)
- Lin J. 1999 Control of turbulent boundary-layer separation using micro-vortex generators. In 30th Fluid Dynamics Conf. Reston, VA: AIAA.
- Storms BL, Jang CS. 1994 Lift enhancement of an airfoil using a Gurney flap and vortex generators.J. Aircr. 31, 542–547. (doi:10.2514/3.46528)
- Myose R, Papadakis M, Heron I. 1998 Gurney flap experiments on airfoils, wings, and reflection plane model. J. Aircr. 35, 206– 211. (doi:10.2514/2.2309)
- Wang JJ, Li YC, Choi K-S. 2008 Gurney flap—lift enhancement, mechanisms and applications. Prog. Aerosp. Sci. 44, 22 – 47. (doi:10.1016/j.paerosci.2007.10.001)
- Guerrero JE, Maestro D, Bottaro A. 2012 Biomimetic spiroid winglets for lift and drag control. Comptes Rendus Me´canique 340, 67 – 80. (doi:10.1016/j.crme.2011.11.007)
- Whitcomb RT. 1976 A design approach and selected wind-tunnel results at high subsonic speeds for wing-tip mounted winglets. Hampton, VA: NASA Langley Research Center.

Thank you

- Prawin